Microfluidic system

Master thesis

Stefan Johansen, 5MC

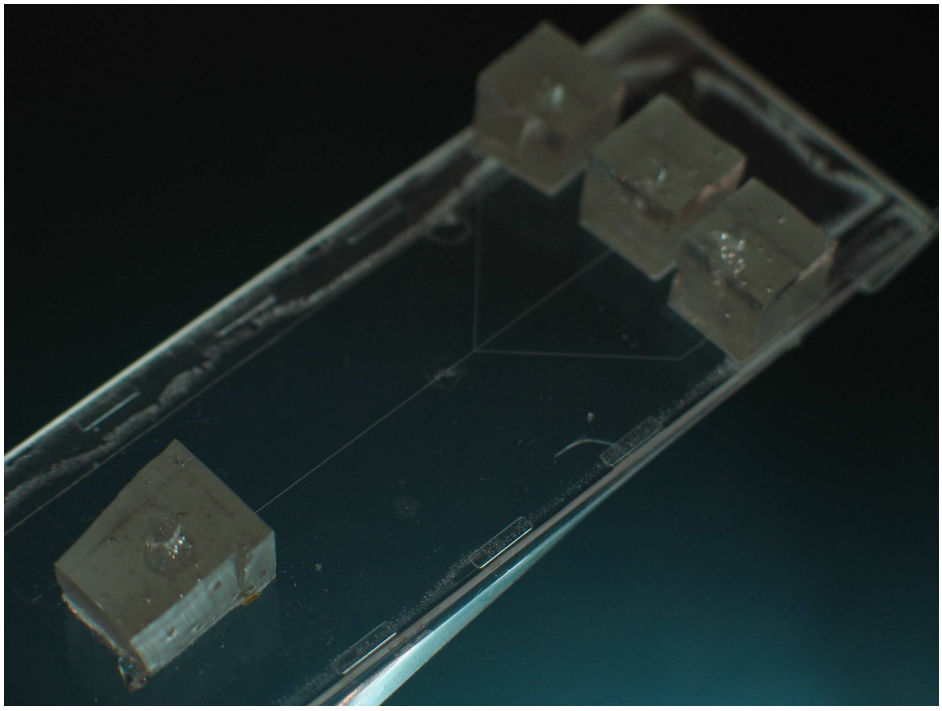

Supervisors: Ralf Frese, Horst-Günther Rubahn

NanoSYD, SDU, spring 2009

Contents

Preface

Upon studying engineering within the field of electronics, software and macro-scaled mechanics for a total of three and a half years, an elective course giving an introduction to fundamentals of nanotechnology became part of the curriculum. This course was the first eye-opener into a whole new world, which has become a greater interest ever since. Research within the field of nanotechnology came to the city of Sønderborg with the initiation of University of Southern Denmark's new campus – Alsion. Until then, NanoSYD had been situated at the campus in Odense. As cleanroom facilities were included in the building of Alsion, it became relevant to move the nanotechnology research here, and it became relevant for the engineering studies in Sønderborg to include a nano-profile.

Being part of the very first class of master's students to be matriculated at the new facilities has shaped the past 2 years in many ways. New buildings mean new routines, and incorporating a whole new research area into an existing array of study plans, lectures and other research is a large task. As student during this period it has been valuable to be welcomed as member of the research group – being asked to participate in group meetings and experience the sharing of results and knowledge on equal terms with professors, post doctorates and PhD students has been a very nice experience. A thank you is owed to the group members for their support – feeling like a colleague more than a student makes work a fun experience.

It is my hope that future engineering students in Sønderborg will benefit from the research at NanoSYD even more than I have. I can strongly support the effort of incorporating basic theoretic courses earlier in the education, letting the bonds between research and industry grow, in turn seeing new products brought to market as a result of the research.

During the course of work on this project, I have enjoyed sparring with Ralf Frese – not merely a supervisor, but also a mentor in the world of research. Thank you for guiding me in the right directions along the way, and for pushing me to believe in success even when I found it difficult.

A special thank you also goes to Horst-Günther Rubahn and Jakob Kjelstrup-Hansen, for counseling regarding the project and my plans for the future. Whether I continue in the world of academia or elsewhere is still uncertain, but I know where to go for help.

Thank you also to Casper Kunstmann-Olesen for helping with experiments and equipment setup.

Finally I would like to extend a thank you to Bjarke Jacobsen, for great cooperation in the parts of our projects where we could work together, and for cooperation along the way. 5 years of studying together are coming to an end, but I hope the friendship we share has only just begun.

Sønderborg, June 02, 2009

_____

Stefan Johansen

1. Project background

1.1. Project description

The European Union supports a programme intended to stimulate and develop potentials across nationalities and boundaries. This project, Interreg, has many sub-programmes centered on border regions between 2 or more countries. The purpose of these programmes is to promote local cooperation between research institutions and industry across regional borders, by supporting research and development projects. One such project is titled “Lab-on-a-chip technology for quality control in the foodstuff- and bio-industry” (translation of the Danish title from [1]). It belongs in the Interreg4A region, consisting of Southern Denmark, Schleswig and the K.E.R.N. area in Germany.

The Lab-on-a-chip project is organized in collaboration between researchers from the University of Applied Sciences in Flensburg, the University of Applied Science at Fachhochschule Kiel and NanoSYD from the University of Southern Denmark in Sønderborg. It was initiated in September of 2008 and will go on until the end of August 2011. The purpose of the project is to develop a lab-on-a-chip device for quick sample analysis with the purpose of identifying and quantifying certain types of cells that can occur in food production or other biological processes. Today this is often done by manually taking out samples in the production, and performing different analysis. As this is a time-consuming process, requiring specialized instruments, it would be a large benefit for the industry if tests could be performed quicker and easier. Research on NanoSYD’s part of the Lab-on-a-chip project is undertaken by Casper Kunstmann-Olesen, a Ph.D. student on the project.

Flow cytometry is a method for analyzing cells in a suspension. A solution of cells is subjected to hydrodynamic focusing in order to achieve a “string” of individual cells, which is then in turn analyzed. Analysis is typically performed using a laser to illuminate the individual cells, and an array of sensors to detect scattered and emitted light as well as fluorescence. The object of the Interreg project is to minimize the size of this process onto a single chip, and in turn eventually implement further detection methods to broaden the field of applications.

The project at hand is focused on developing a prototype to investigate the focusing of a suspension, in practice by creating a microfluidic channel system for hydrodynamic focusing in a polymer sample. It is the final project in a Master’s study, and is thus limited to a workload of 30 ECTS points (1 semester’s full time work).

My educational background is within the field of Mechatronics engineering, giving a practically oriented approach to the thesis work. Due to the time and work constraints governing the project, the focus is on the channel system alone, as the cytometry measurements and analysis are part of the bigger Lab-on-a-chip project. The project is an individual performance, however closely related to that of a fellow student, Bjarke Jacobsen, who has the same educational background and is performing a similar task during his thesis work. The focus of Bjarke’s work is to create a similar focusing system, but using standard lithography methods to produce it in silicon. The equal nature of the two projects enables performing common measurements and analysis on commercially available focusing systems, as well as comparing the achieved results. This should be an aid to the researchers

on the larger project to determine what production method is most feasible for the actual cytometer chip.

Prior to the beginning of the Master's thesis, an initial project has been performed during the last semester of lectures. The purpose of this project was to get acquainted with fundamental laboratory work, operation and control of the Excimer laser, and gain experience working with different characterisation and measurement equipment in the cleanroom and surface laboratory at NanoSYD. This project gave a valuable insight into the research world, and background knowledge necessary for taking on a project which in many ways is different from previous projects during the Mechatronics studies.

1.2. Project aims

Hydrodynamic focusing is desired to enable flow cytometry analysis of cells in a suspension. The purpose of the project is to:

- Test and analyze focus capabilities of commercially available focusing system acquired from Microfluidic ChipShop GmbH
- Produce prototype of system for hydrodynamic focusing in polymer material
- Investigate sealing methods and interfacing to produced prototype
- Be able to control focus width between 1 and 10 µm
- Compare prototype to commercial system, and to prototype created in silicon in parallel project

Production is to be performed using an ArF excimer laser, and experiments should be conducted to determine the production parameters. Production time as well as reproducibility should be evaluated and compared to that of the parallel project.

2. Background principles

2.1. Lasing

To understand the principle of lasing, one must first understand the principles of light. The smallest building blocks of our world are the atoms. An atom consists of a core, containing protons and neutrons, and around this core a number of electrons revolve – much like the moon around the planet earth, or the planets around the sun.

The electrons can have different energy levels with respect to the core – this can be seen as an energy potential. There are a discrete number of possible energy levels around the atomic nucleus, known as shells, in which the electrons must be. The outermost electrons around the nucleus, called the valence electrons, are movable – when in their "ground state", they are in the unoccupied shell closest to the nucleus. However, atomic collisions, electron collisions, photon absorption or electromagnetic energy can make an electron jump to a higher energy level. When an atom has an electron in a level higher than the ground level, it is known as an excited atom. This is only a temporary state, and after a short time (around 10 ns), the electron returns to its ground state. In order to do that, it must get rid of the excess energy – and this happens by emission of a photon, whose energy is given by the Einstein equation [2]:

$$E = hf = \frac{hc}{\lambda} \qquad \textbf{(2-1)}$$

Where *c* is the speed of light, *f* is the frequency of the emitted photon, λ is the wavelength of the emitted photon and *h* is known as Planck's constant ($6.626 \cdot 10^{-34}$ J·s = $4.136 \cdot 10^{-15}$ eV·s).

As Einstein's equation shows, the frequency of the emitted photon is inversely proportional to its wavelength – the shorter the wavelength, the higher the frequency – and the higher the energy. The photon energy is equal to the potential difference between the excited level in which the electron starts and the relaxed level it jumps to.

The different energy levels around the nucleus of a specific atom determine the wavelengths of the photons this element can emit.

When an atom is subjected to an external force, such as an electromagnetic field or being hit by a photon, one of a number of things can happen. If the photon hitting an atom in its ground state has less energy potential than the difference between the ground state and the next, higher state of the electron, no excitation can take place. Instead the photon is scattered, meaning that it will continue in an arbitrary direction away from the atom again. Its energy is the same, which is why this process is known as elastic scattering.

If the energy of an incoming photon exactly matches the energy gap between the electrons current state and a higher state, it can result in what is known as Resonance absorption – the photon is absorbed, and the electron jumps to a higher energy level. After this has happened, a number of things can take place:

If enough time passes, Spontaneous emission of a photon will take place as the electron returns to its ground state. This can happen directly, emitting only one photon with the same wavelength and energy as the one moving it to the higher state, or through a series of jumps between intermediate-energy states, resulting in a number of longer-wavelength photons being emitted.

For most materials spontaneous emission will occur shortly after the excitation – however some materials can stay excited for much longer time before relaxing and emitting light. The excited electrons in these materials are said to be in a metastable stage, and the materials are known as phosphorescent.

For some materials, absorption of a photon can result in an electron being emitted from the atom, thus ionizing it. This is known as the photoelectric effect, and is the basic principle employed in solar cells.

In the event where an atom is already in an excited state and an incoming photon holds exactly the same energy potential as that between the excited electron and a lower energy shell, a process known as Stimulated emission can take place. The electron will decay to the lower energy state, and emit a photon which has the same phase and wavelength as the incoming photon, and is emitted in the same direction. Under the right circumstances this can result in an amplified “ray” of photons travelling in the same direction, and this is the fundamental principle in a laser.

The word “LASER” is an acronym for “Light Amplification by Stimulated Emission of Radiation”, and a laser principally requires two things to operate. Lasing takes place in what is known as an optical resonator, made from two mirrors facing each other. One of these mirrors reflect 100% of the incoming photons of the desired wavelength, the other mirror lets a small percentage pass. Between these mirrors are placed the active medium, in which the stimulated emission can be achieved.

If no external forces are applied, electrons will decay towards their ground state. When the system is in thermal equilibrium, the number of electrons in an excited state (N_2) versus the number of electrons in the ground state (N_1) will be governed by a Boltzmann distribution, with the most electrons in the ground state.

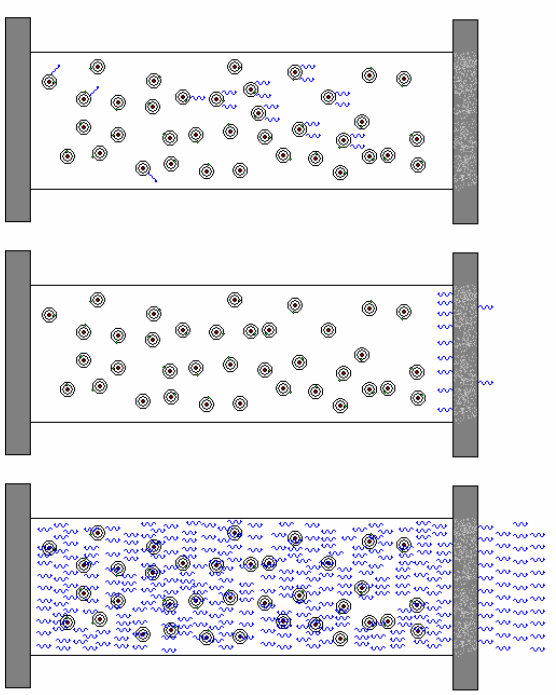

Figure 2-1 - Laser resonator principle

If an external force is applied (an electromagnetic field, light shining on the medium or other forces), some electrons can be excited. For lasing to take place, there has to be more excited than relaxed atoms, known as "population inversion". Achieving this is called optical pumping. For amplification to take place, a minimum of 3 energy levels is required (E_1, the ground level, E_2 and E_3, the excited levels). Initially, the number of atoms in the relaxed state (N_1) is much larger than the number of excited atoms. When the external force is applied, a number of electrons are excited to the higher state E_3, from which they drop to the metastable state E_2. When they return to the ground state E_1, they emit photons. These photons can either generate stimulated emission in other excited atoms in the E_2 state, or excite relaxed atoms from state E_1 to E_2. If population inversion is achieved due to the external force ($N_2 > N_1$), it is more likely for a photon to meet an excited atom and generate stimulated emission, and light amplification is realized. Figure 2-1 illustrates the working principle of the resonator, once population inversion is achieved. In the top image, a series of photons are emitted in arbitrary directions from the excited atoms. Those that on the way encounter other excited atoms will cause spontaneous emission from these, causing light amplification. Once the semi-transparent mirror is reached, as shown in the middle image, most of the photons are reflected, while a few are passing through. In the bottom image the situation a little later can be seen, in which a lot of stimulated emissions have happened, and a beam of light is emitted from the resonator.

Most modern lasers operate with at least 4 energy levels – a ground state E_1 and 3 excited states E_2, E_3 and E_4. The state E_3 is metastable, meaning that the electrons can stay here for several ms, whereas the transitions from state E_4 to E_3 and from state E_2 to E_1 take place almost immediately upon excitation. Initially, the total number of valence electrons in the system is presumed to be in the ground state ($N1 \approx N$, $N2 \approx N3 \approx N4 \approx 0$). This means that as soon as electrons begin to get excited to the state E_4 and drop to E_3, a population inversion is built up with respect to E_2. When the first

electrons spontaneously decay from E_3 to E_2, the photons can interact with other excited atoms, and stimulated emission occurs, causing amplification of the light.

The characteristics of the amplified light wave are that the photons are:

- Coherent (All in phase with each other).
- Monochromatic (All have the same wavelength).
- Collimated (Due to the parallel mirrors, all photons that "escape" the resonator travel in the same direction).

2.1.1 Excimer lasers

Excimer lasers are characteristic by the fact that the active lasing medium is a gas mixture enabling the formation of excited dimers or excited complexes; the word "excimer" is used to describe either. Excimers have been used to achieve lasing in wavelengths between 126-600 nm [3].

An excimer molecule consists of a rare-gas and a halogen atom. A rare-gas is inert, as it has 8 electrons in its valence shell. It can however be brought to a metastable excited state, in which one electron moves to an outer shell; whilst in this state, it can perform a compound with a halogen. Due to the halogen's nature, it forms very strong bonds. After a period of time the metastable rare-gas molecule returns to its ground state and the bond between the atoms are broken as a photon is emitted. The atoms repulse each other, and return to their ground state immediately upon relaxing of the excited rare-gas atom and photon emission. Population inversion is achieved as soon as the first excimer molecule is formed, and with the atoms returning immediately to their ground states, subsequent excitation and reaction can take place more or less continuously. In order to bring the rare-gas atoms to their excited state a high energy density is required, achievable by very fast switching of a high current [4]. Due to this high energy requirement, excimer lasers can only be operated in pulsed mode.

The excimer laser used in this project is run with Argon as the rare-gas and Fluorine as the halogen. They are added to the reaction chamber in a ratio of approximately 1,5 % Ar, 0,5 % F and the remaining 98 % of the mixture consists of Neon as a buffer gas. Fluorine is one of the most reactive of all the elements, and is very poisonous, so care must be taken to handle it correctly.

The ArF excimer laser emits photons with a wavelength of 193 nm, corresponding to an energy of 6.4 eV. It has a low spatial and temporal coherence, but a high power, and due to the short wavelength it can be focused down to very small sizes, resulting in a very high intensity.

2.2. Laser units and calculations

When using a laser to ablate structures in polymer samples, it is nice to be familiar with the units and relations in the world of lasing. A laser beam principally consists of a collimated row of photons with the same wavelength and phase. In a pulsed laser the pulse has a duration of τ [s], and a total energy of E_p [J] . A given area subjected to the laser pulse is said to have been subject to an irradiation I given by:

$$I = \frac{E_p}{A \cdot \tau} \quad \left[\frac{W}{cm^2}\right] \tag{2-2}$$

Irradiation of a surface area dA over time results in accumulation of laser energy, known as fluence:

$$F = \int I \, dt \quad \left[\frac{J}{cm^2}\right] \tag{2-3}$$

A surface subjected to a pulsed laser working with a pulse frequency of f_p, during a period of time t, is said to have been subjected to an "irradiation dose" of:

$$D = F \cdot t \cdot f_p \quad \left[\frac{J}{cm^2}\right] \tag{2-4}$$

The irradiation dose on the surface of a sample mounted in the laser production setup can be calculated using a series of measurements. First of all, the output energy of the laser must be determined. For this purpose a Joule-meter can be placed in the laser path, being subjected to the energy from the laser pulses. Here it is worth noting that an excimer laser typically has an inhomogeneous beam profile, but for the calculations it is assumed to be homogenous.

A Joule-meter outputs a voltage directly proportional to the influx of the laser light, observable on an oscilloscope. For performing the following set of calculations, measurements were performed on the laser setup when working on prototype production, using two differently scaled Joule-meters. The outputs showed quite different values, but calculations are simply performed for both measured values.

In order to determine the irradiation, the area of the sample surface subjected to the laser pulses as well as that of the mask is needed in order to determine the magnification factor.

Mask dimensions		Sample surface dimensions	
Width	Height	Width	Height
1500µm	750µm	60µm	30µm
0,15cm	0,075cm	0,006cm	0,003cm
Aperture area		Aperture area	
0,01125cm^2		0,000018cm^2	
Area magnification factor			
625			

In order to calculate the fluence on the sample surface, the readings from the Joule-meters must be converted to the right units:

Laser power measurements		
Joulemeter scaling	2,3V/J	8,3V/J
Measured value	40,8mV/Pulse	106mV/Pulse
Equal to	0,0408V/Pulse	0,106V/Pulse
Corresponding to	0,01773913J/pulse	0,012771084J/pulse

The measured values of energy per laser pulse is now known, but in order to determine the fluence on the sample surface only the amount of light that reaches the sample should be counted. The measured value covers the whole laser spot size, but only a fraction of this actually passes the aperture. The spot size of the laser is approximately 20x20 mm, and calculations estimate the fluence on the sample surface to be:

Laser beam size 2x2 cm	4cm^2	4cm^2
Fluence on mask	0,004434783(J/cm^2)/Pulse	0,003192771(J/ cm^2)/Pulse
Aperture area	0,01125cm^2	0,01125cm^2
Fluence through aperture	4,98913E-05(J/cm^2)/Pulse	3,59187E-05(J/cm^2)/Pulse
Equal to	0,049891304mJ	0,035918675mJ
On the focused spot	31,18206522mJ/Pulse	22,44917169mJ/Pulse

Apparently the laser energy is between 22,4 and 31,18 mJ per pulse on the focused spot of 30x60 µm. This corresponds to a value of between approximately 1,247 and 1,732 kJ/cm^2, or an irradiation dose between 62,3 and 86,6 kJ/cm^2/s at an operating frequency of 50 Hz.

2.3. Polymer ablation

Polymer materials in general consist of monomer molecules – long chains, connected to each other in a seemingly random fashion. As such, polymers have no grid structure, and strength properties tend to be the same in all directions. In this project a polymer has been used that is called PolyMethylMethacrylate, or PMMA. Its chemical composition is $(C_5O_2H_8)n$, the n denoting one or more similar neighboring molecules, used to form the long chains.

When a PMMA sample is subjected to excimer laser fluence, a part of the sample surface is struck by a large quantity of photons with energy of approximately 6.4 eV. each. As a photon encounters the sample surface, a reaction takes place. Typically a surface molecule is his by the photon, and the power transferred can either cause scattering, vibration or bond breaking. As the excimer photons are very energetic, they are in many cases are stronger than the bonds holding the monomers together. This is also the case for PMMA, with a binding energy of 2.7 eV [4]. As the photon interfaces a monomer, it is knocked loose from where it sits, but as this requires less energy than the photon arrived with, the remaining energy can be transformed into breaking the monomer into its compounds. Ordinarily, however, the energy is transferred into movement energy of the monomer, accelerating it up to a speed that is determined by:

$$v = \sqrt{\frac{2E_{ex}}{m}} \qquad \textbf{(2-5)}$$

Where m is the mass of the PMMA monomer (8.3×10^{-25} kg), and

$$E_{ex} = E_{ph} - E_B \qquad \textbf{(2-6)}$$

The monomers binding energy is denoted by E_B, and the energy of the photon is called E_{ph}. The previous equations determine a movement velocity of approximately 1200 m/s **[4]** of the MMA monomers due to excess energy from the photon upon ablation.

Figure 2-2 illustrates the principle of ablation with an excimer laser. Especially important to notice on this figure are the two images in the centre. On the second image from the left the substrate initially absorbs energy from the laser pulse, but no ablation is taking place. So-called threshold fluence can be observed when experimenting with polymer ablation – the first photons to strike the surface do not induce ablation, but rather prepares the surface for ablation by the next pulses. Since the ArF excimer has very high photon energy, the threshold fluence is not as high as for longer-wavelength lasers, and ablation is mainly governed by nonthermal ablation.

Ablation with lasers in the UV range consists of longer-wavelength photons, and a significant portion of the photon-sample interaction takes place below the threshold fluence. This causes vibrational heating between the molecules, in turn heating the material and thus ablating it. This process is known as thermal ablation, and is characterized by a high throughput and continuous laser-operation, but with samples visibly and structurally affected by massive heating, resulting in charred and deform edges around the ablated structures.

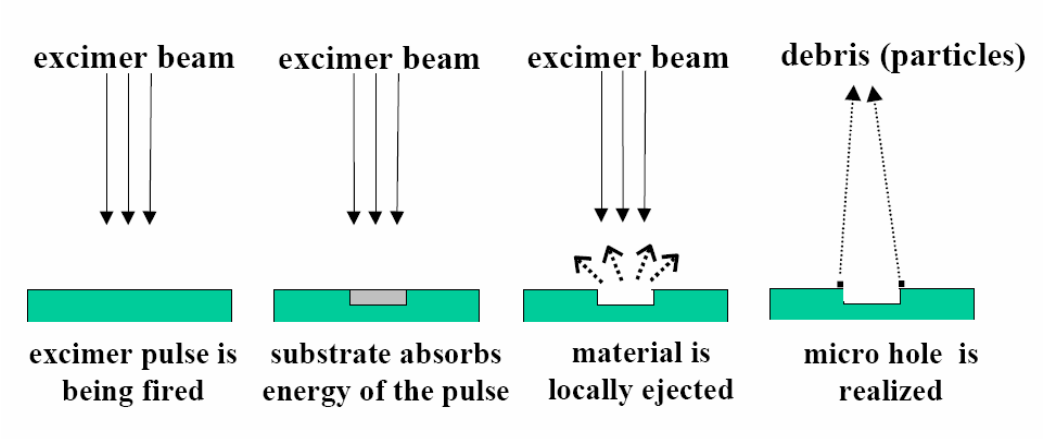

Figure 2-2 – Laser ablation principle

Source: [5]

The third picture from the right on Figure 2-2 shows ejection of material, as the threshold fluence has been surpassed. A characteristic observation during experiments with ablation of PMMA and other polymers is that ejected monomers and other debris form a "plume" – a balloon-shaped cloud above the focus spot partially blocking the laser. This material can disturb the ablation process as interactions between the photons and the particles in the air are likely to take place. Also, the debris is likely to return to the sample surface, or perhaps to the previously ablated structures, where it can reattach or in other ways change the surface properties.

2.4. Reynolds number

The Reynolds number is a dimensionless quantity, defined by the relationship between inertial and viscous forces in a channel system:

$$Re = \frac{\text{Inertial forces}}{\text{Viscous forces}} = \frac{V_m \cdot D}{\upsilon} = \frac{\rho \cdot V_m \cdot D}{\mu} = \frac{Q \cdot D}{\upsilon \cdot A} \qquad \textbf{(2-7)}$$

Where:

V_m = mean flow velocity [m/s]

Q = channel flow [m^3/s]

D = hydraulic diameter [m]

$\upsilon = \mu / \rho$ = kinematic viscosity of the fluid [m^2/s]

A = channel cross-sectional area [m^2]

The value of the Reynolds number determines whether the flow in the channel is turbulent, transitional or laminar. In case of high Reynolds number (Re>4000), flow is normally turbulent – inertial forces dominate and the fluid expresses random fluctuations. The fluids from two or more channels with Re>4000 intersecting into a common channel will be completely mixed almost immediately.

Transitional flow takes place when the Reynolds number is between 2300 and 4000. The flow in the channels switches randomly between laminar and turbulent flow.

For Reynolds numbers below 2300, the flow is normally always purely laminar – viscosity is the dominating force, and mixing of 2 or more liquids happen only through diffusion.

Calculating Reynolds numbers requires calculating the hydraulic diameter of the channel. This is given as [6]:

$$D = \frac{4 \cdot A}{p} \qquad \textbf{(2-8)}$$

Where p is the perimeter of the channel. For rectangular channels the hydraulic diameter can be expressed also as $D = 2 \cdot h \cdot w / (h+w)$, with h being the channel height and w its width.

A microfluidic channel with dimensions of 500x500 µm and a flow of water of 500 µL/min has a hydraulic diameter D of $0{,}5 \cdot 10^{-3}$ and a Reynolds number of 18,69. Dimensions in the micrometre range generally result in very low Reynolds numbers, so systems on this scale can be expected for all microfluidics flow to be purely laminar. (Kinematic viscosity of water at 20°C found in [2]). Due to the low Reynolds number of microfluidic systems such as those produced in this project, purely laminar flow is expected.

2.5. Focus width model

Hydrodynamic focusing taking place in a channel system can be modelled in different ways. A simple model, subject to a number of assumptions, has been used to predict the width of the focus stream as function of the input volumetric flows, and in turn develop a scheme for making comparable measurements across different channel systems.

Assumptions are as follows:

i. Newtonian fluids, with equal density in all channels

ii. Laminar, steady flow

iii. Flow is pressure driven

iv. Channel heights are equal throughout the system

v. Output flow velocity is estimated equal across channel width

h Height of channel [µm]

Q_i Volumetric flow rate of the sample inlet channel [µL min^{-1}]

Q_o Volumetric flow rate of the outlet channel [µL min^{-1}]

Q_s Volumetric flow rate of each of the side channels [µL min^{-1}]

V_f Velocity averaged across focus stream

V_o Velocity averaged across outlet channel

w_f Width of the focused stream [µm]

w_o Width of the outlet channel [µm]

w_i Width of the inlet channel [µm]

w_s Width of the side channel [µm]

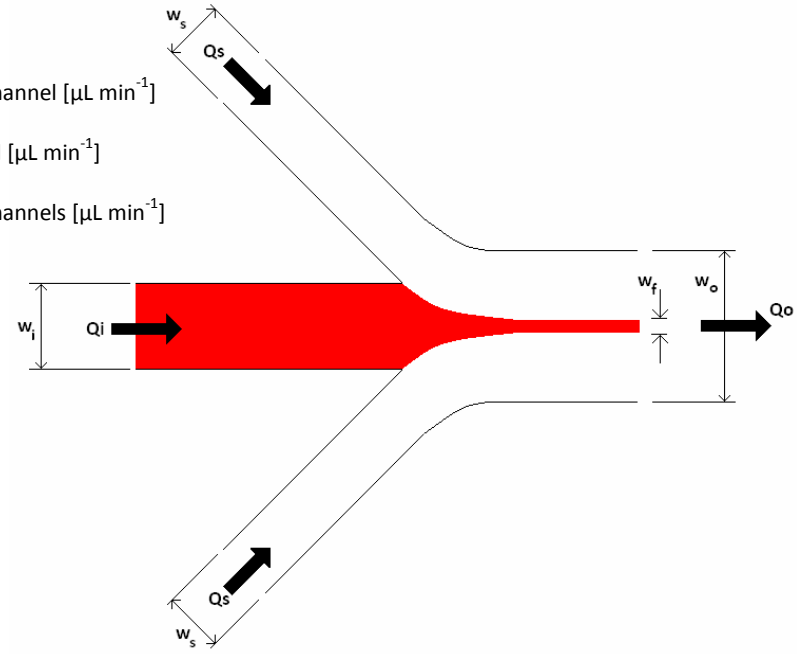

Figure 2-3 - Model definitions

Definitions of the model variables can be seen on Figure 2-3. The volumetric flow rates of the inlet channels are directly controllable, and according to the principle of mass conservation the amount of fluid pumped through either inlet channel must equal the amount of fluid passing through the equivalent stream of the outlet channel.

The total flow in the focused stream must equal the total flow in the sample input channel

$$Q_i = w_f \cdot h \cdot v_f \tag{2-9}$$

The total flow of fluid passing through the outlet channel equals the sum of the input channels

$$Q_o = w_o \cdot h \cdot v_o = Q_i + 2 \cdot Q_s \tag{2-10}$$

In order to determine the width of the focused channel, the previous equations are combined

$$w_f = w_o \frac{Q_i}{\frac{V_f}{V_o} \cdot (Q_i + 2 \cdot Q_s)} \tag{2-11}$$

As comparison between different systems, with different output channel widths, is required, the equation is rearranged to give the focus width with respect to this. According to assumption v., the flow velocity is estimated to be equal across the entire width of the channel, making V_f equal to V_o, so this ratio can be ignored. The remainder of the equation is simplified to give the following relation between output channel width and focus width:

$$\frac{w_f}{w_o} = \left(\frac{2 \cdot Q_s}{Q_i} \right)^{-1} \tag{2-12}$$

In order to be able to test a series of different prototypes, with different dimensions, the equation derived above was used to calculate the values to be used in the experiments. Early tests made on the commercially available system indicated that the focused flow was indeed directly proportional to the ratio between Q_i and Q_o. When keeping the ratio constant, the resulting flow focus also remained constant – however if Q_o became too small, the lower speed of the fluorescent fluid made contrast on measurement images much lower. A treshold value for Q_o was determined, and included in a model for calculating measurement settings.

Both parallel projects had as a goal to be able to control the width of the focus channel between 1 and 10 µm. A series of values was devised to attempt reaching 10 different widths on each system. The 9 values ranged from 2 to 30 µm, with the final measurement always being ⅓ of the channel width.

Output channel width W_o **60** µm	Total output flow Q_o **150**		
Desired width	Ratio W_f/W_o	Sheath flow Q_s	Sample flow Q_i
2 µm	3,33 %	72,5 µL/min	5,00 µL/min
4 µm	6,67 %	70 µL/min	10,00 µL/min
6 µm	10,00 %	67,5 µL/min	15,00 µL/min
8 µm	13,33 %	65 µL/min	20,00 µL/min
10 µm	16,67 %	62,5 µL/min	25,00 µL/min
15 µm	25,00 %	56,25 µL/min	37,50 µL/min
20 µm	33,33 %	50 µL/min	50,00 µL/min
25 µm	41,67 %	43,75 µL/min	62,50 µL/min
30 µm	50,00 %	37,5 µL/min	75,00 µL/min
20 µm	33,33 %	50 µL/min	50,00 µL/min

Figure 2-4- Experiment model output for 60 µm channel system

All values of Q_s, Q_i and Q_o were calculated with respect to the entered w_o, and ratios to achieve the desired values was plotted directly for use when performing the tests. In order to be able to compare results directly, the desired w_f as a percentage of w_o was also calculated and plotted. The tables on Figure 2-4 and Figure 2-5 are two examples of the output values of the model for different output channel widths W_o.

Output channel width W_o **100** µm	Total output flow Q_o **250**		
Desired width	Ratio W_f/W_o	Sheath flow Q_s	Sample flow Q_i
2 µm	2,00 %	72,5 µL/min	5,00 µL/min
4 µm	4,00 %	70 µL/min	10,00 µL/min
6 µm	6,00 %	67,5 µL/min	15,00 µL/min
8 µm	8,00 %	65 µL/min	20,00 µL/min
10 µm	10,00 %	62,5 µL/min	25,00 µL/min
15 µm	15,00 %	56,25 µL/min	37,50 µL/min
20 µm	20,00 %	50 µL/min	50,00 µL/min
25 µm	25,00 %	43,75 µL/min	62,50 µL/min
30 µm	30,00 %	37,5 µL/min	75,00 µL/min
33 µm	33,33 %	33,333 µL/min	83,33 µL/min

Figure 2-5- Experiment model output for 100 µm channel system

.

The desired channel widths shown in the graphs are meant to be up to one third of the channel width, but with the highest common value of 30 µm, a 60 µm prototype should be tested all the way to a focusing width of 50 %.

2.6. Resistor equivalent circuit

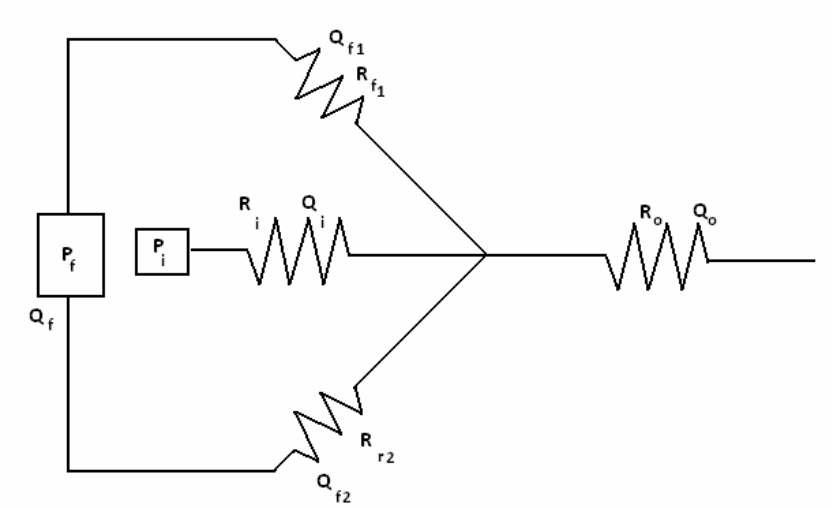

Figure 2-6 - Analogous circuit for pressure drop analysis

In [7], Stiles et al describes a circuit analogous design as the one displayed on Figure 2-6, for analyzing the pressure drop across the system channels. The fluidics equivalent of Ohm's law is described, in which it is stated that:

$$\Delta P = Q \cdot R \tag{2-13}$$

With *ΔP* denoting pressure drop, *Q* is the volumetric flow, and *R* is known as the flow resistance. The value of *R* is dependent on which flow-profile that is assumed in the channel system. In the simple model employed for flow predictions the flow profile was believed to be constant, and the no-slip boundary conditions were neglected. For prototypes such as the ones produced in the project at hand, non-compressible Newtonian fluids are assumed. For pressure-driven flow, the flow profile will have a parabolic shape due to the boundary conditions, also known as Poiseuille flow.

The Poiseouille flow for circular tubes is governed by Poiseuille's law. For rectangular channel cross-sections it can be shown to be expressed as [7]+[8]:

$$\Delta P = \frac{12 \cdot \eta \cdot L}{W \cdot h^3} Q \tag{2-14}$$

Where *L* is the channel length and *η* is the dynamic viscosity of the fluid. *W* and *h* are the width and height of the channel, respectively. The flow resistances (*R*) have been calculated for the different prototypes that were produced in this project. A table of the calculated values can be seen in appendix [1].

3. Experimental

3.1. Prototype design

Initial design considerations for the prototype system to be produced during the scope of this project were made whilst observing commercially available microfluidic systems. In particular, a system which was acquired in a small quantity for comparative analysis and initial measurements was used as model for the desired prototype. Early in the project phase some tests were performed on this commercial system, and certain observations were made, to be considered whilst designing the prototype. First of all, the production of the commercial system was such that a total of 28 connectors for attaching tubing were placed along the sides of the chip containing the system (Figure 3-1.b). As observations of the systems were made using an optical fluorescence microscope with standard working-distance objectives, these connectors turned out to be obstacles preventing observations. As the layout of the system shows (Figure 3-1.a), only a total of 7 of the connectors were actually in use, so the remaining could be removed to make room for the microscope objectives.

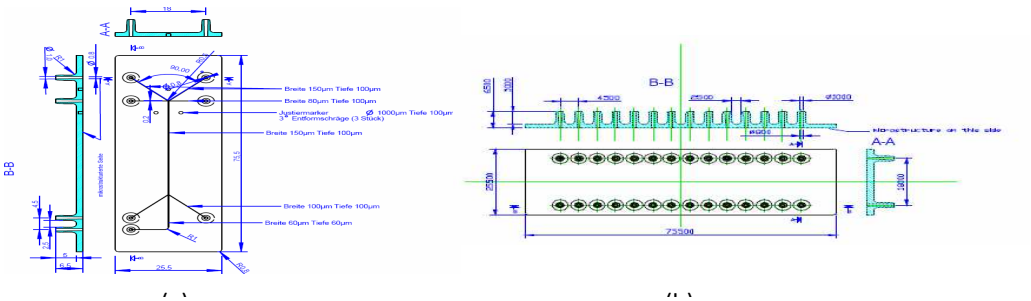

Figure 3-1 – Design of commercial system

(a) – Channel structure and dimensions
(b) – Connector placements on product
Image sources: [9]

As the design of the commercial system also shows, the connectors on the input end of the system (bottom end of Figure 3-1.a) were placed relatively close to the focus point of the system, again giving problems during observations. When designing the layout of the prototype system, these experiences were considered, and the dimensions were made accordingly.

Figure 3-2 shows the initial design for the prototype system. As the prototypes were to be fabricated on PMMA slides the size of standard microscope glass slides (approx. 25,5x75,5 mm, 1 mm thick), the dimensions of course had to be within this range. The most important part of the system was considered the focus point, in which the sample inlet channel and sheath flow channels meet and join the output channel. Observation of this point, and as much of the output channel from the focus point outwards was crucial. Thus, the sheath flow channels were made longer than those on the commercial system. In order to do this, and still remain within the restrictions of the microscope slide, they were designed with an angular deflection approximately 14 mm. from the focus point, in

turn making the total length of the sheath flow channels 4 mm. longer than that of the 15 mm. long sample inlet channel.

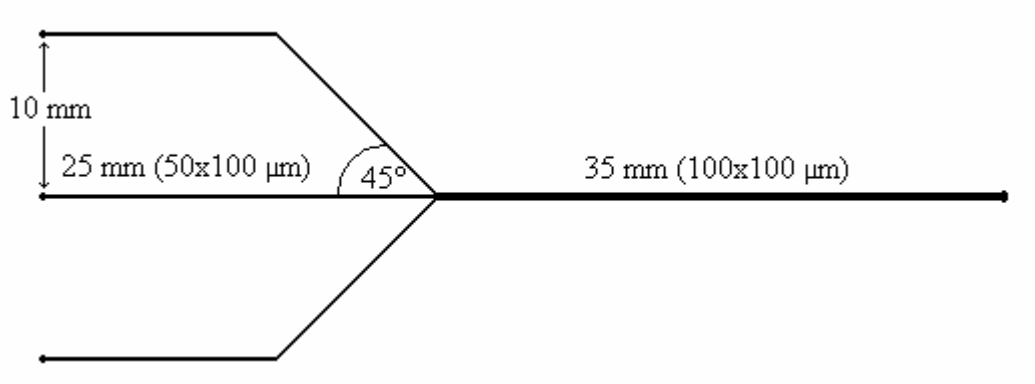

Figure 3-2 – Initial design of prototype system

As the project progressed, the first two prototypes were eventually produced, as will be described in later sections of this document. Due to limitations of the production setup, the achieved channels in the prototype had smaller cross-sectional dimensions than those intended. The first two finished prototypes had dimensions as indicated on Figure 3-3.

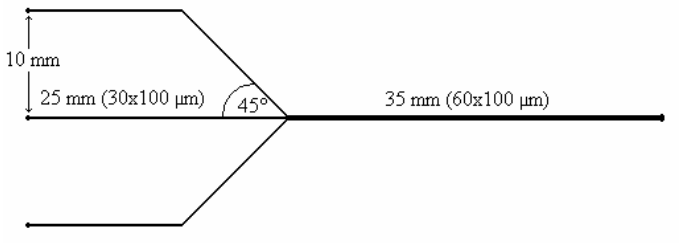

Figure 3-3 – Achieved dimensions on first prototype production

In paragraph 3.4.4 the sealing of the system is described, as well as some obstacles that required a second system design. This design needed to have shorter channels to improve functionality of the finished prototype, and was shortened a total of 20 mm. along the length of the system.

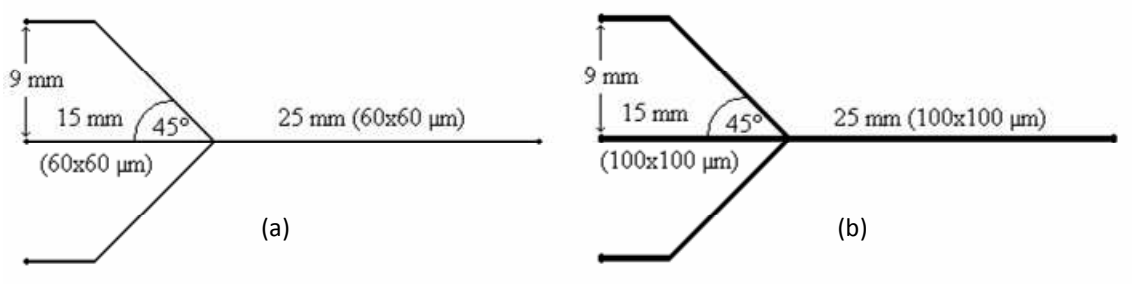

Figure 3-4 – Second prototype dimensions

(a) – Dimensions of 1-aperture prototype #1
(b) – Dimensions of 1-aperture prototype #2

Due to further obstacles also described in paragraph 3.4.4, two final prototypes using a single aperture for the entire production process were made at a later time, with dimensions as indicated on Figure 3-4.a and b.

3.2. Production setup

Production of the microfluidic systems in this project was performed using an ArF excimer laser setup, a sketch of which can be seen in Figure 3-5. In order for such a production to take place, a number of components are necessary. The laser itself outputs a series of pulses, and the beam of light is directed towards the surface of the sample using 3 dichroic mirrors. These mirrors are reflecting 100% of the light at the UV wavelength of the laser, and are transparent in the wavelength area of visible light.

In the laser path, in order to achieve the desired micro structure, a number of items are placed. At first, the beam passes an attenuator. This device is useful in applications where the samples shot are very sensitive to the UV light, and the intensity of the light needs to be attenuated in order to achieve precise control. For PMMA ablation a great number of pulses is needed to achieve the desired channel depth, so attenuating the light has not been necessary.

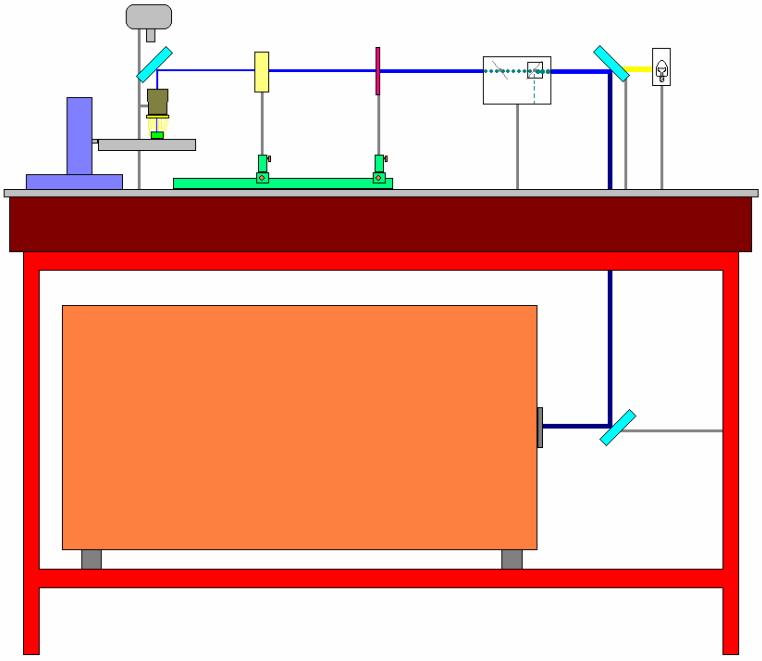

Figure 3-5 - Excimer laser setup

Upon passing through the attenuator, the laser beam next encounters one or more apertures, used to cut out the parts of it not needed for the desired focal point shape. Finally the beam passes a focusing objective, demagnifying the light onto the surface of the sample to be treated by the laser.

The sample is placed on a 3-axis moving stage, controlled by stepper motors, to enable making structures on the surface on the sample by moving it.

In order to be able to observe the sample, a CCD camera is placed directly above it, looking through the last dichroic mirror from above. Two light sources are combined to enable the monitoring of the

sample and the beam shape and position – a dark field illuminating ring around the focusing objective provides general sample light, and a light bulb behind the second dichroic mirror shines light through the attenuator and apertures, enabling the adjustment of these without the laser running.

The projecting lens has a demagnification factor of 15 times. It is a Schwarzschild objective, containing two spherical mirrors. As the second, smaller of these mirrors is held by three small "legs", the resulting laser spot is shaped as depicted in Figure 3-6. In order to ensure an even intensity, the laser spot must fit within one of the segments of this spot, limiting the realizable size to fit within approximately 100x100 µm at most.

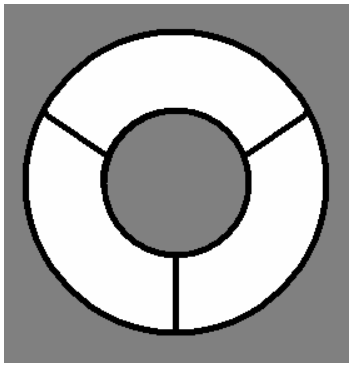

Figure 3-6 – Schwarzschild objective laser spot

To produce a microfluidic channel system with dimensions of centimetres on the length scale, a laser control principle must be employed. One option is to shoot individual spots with a shape defined by the apertures, and then let these shots overlap in order to "stitch" together a long channel. Another option is to let the laser run with a high shot frequency, whilst moving the sample to be ablated in the direction of the desired channel, resulting in a long line, equally ablated at all places, in this document referred to as "line ablation". In order to realize a channel with a rectangular cross-section, the fluence along the width of the channel must be equal during the processing. This can be realized when moving the sample along one of the axes of a rectangular aperture, making patterns consisting of perpendicular lines the easiest realizable structures.

When the desired structures are no longer perpendicular channels, the only way to ensure a uniform fluence along the line is by utilizing an angled rectangular aperture. The most feasible way of realizing such an aperture is by designing a mask to insert in the beam path.

3.3. Mask design

Masks are widely used in microfabrication, especially in lithography processes, so software for designing masks is available from numerous sources. For this project the program LayoutEditor was selected, since it was found to be a versatile tool, intuitively usable, and come with a licence that allowed usage for non-commercial purposes at no cost. The design of the mask was made to enable as diverse a production as possible (Figure 3-7). It was desired to be able to experiment with different channel widths as well as different angular intersections.

A mask like the one ordered is made on a 5 inch square glass, in this case pure Quartz to ensure transparency at a wavelength of 193 nm[1], and has a user-definable area of 100x100 mm. In order to be able to focus on only one "aperture" at a time, and easily find the desired pattern, this area was split into 81 10x10 mm. squares, each labelled according to their row and column, and in the centre of each of these squares was placed one shape. The scale was made 15:1, in order to match the 15 times projecting lens above the sample. Due to the maximum realizable size of the laser spot, no structures could be made that were intended to reach outside a 100x100 µm square.

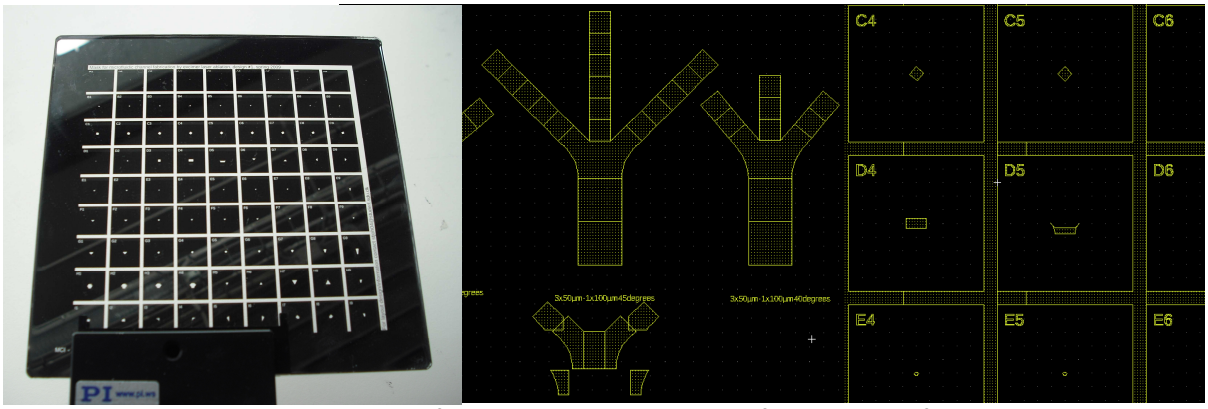

Figure 3-7 - Mask for line ablation, with details from layout software

Operation of the production process was intended to be semi-automated, as the scope of the project is prototype production only. As such, each aperture of the mask has to be manually adjusted to the right position as part of a step-wise "stitching" production. In this, each shape is used one or more times for creating either single shots or long lines, all intersecting in one place – the focus point of the channel system.

In practical application, it was not possible to achieve the desired sizes of the apertures from the mask. When producing systems that require the use of more than one aperture, exchange and adjustment of the apertures between production steps is crucial. This is made possible by the visual feedback from the camera attached to the computer controlling the laser production system.

[1] Mask data sheet describing the substrate specifications can be seen on appendix 2

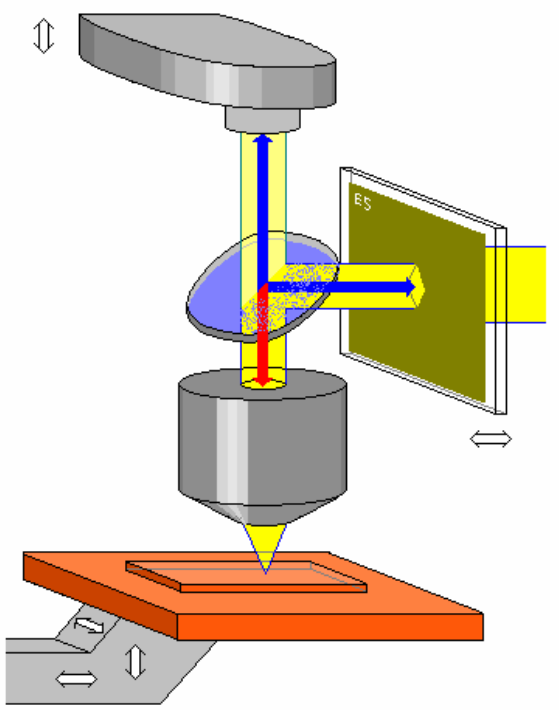

Figure 3-8 - Mask + camera alignment

When adjusting an aperture, the surface of the sample to be produced is first brought into the focus of the camera by adjusting the z-axis of the sample stage. Then the mask is adjusted, in order to move the desired aperture to the correct position within the ablation area (the active area of the Schwarzschild laser spot, as seen on Figure 3-6). The focus of the aperture on the sample surface can be adjusted by moving the mask closer to or further away from the projection lens. In Figure 3-8 the distance between the projection lens and the camera lens is illustrated by the red/blue arrow crossing the dichroic mirror, and as the arrows indicate, this distance is equal to that between the projection lens and the mask. This ensures that the aperture from the mask is in focus on the surface of the sample to be ablated when the surface is also in focus on the CCD chip of the camera, and thus visible in the control software.

Altering the distance between the mask and the projection lens will affect the size of the focused aperture – but at the same time requires a change in focus in order to produce sharp, well-defined edges of the ablated channels. For the sequential, “stitching” prototype production, it is essential that the surface is in focus on the image from the camera, so the different apertures can be adjusted with respect to each other and remain inside the active area of the laser beam. In the actual production setup that has been used for this project, the physical limitations of the possible adjustments resulted in the focused aperture to have dimensions of approximately 60% of the desired dimensions. Moving the mask in order to change the size required simultaneously moving the camera in order to keep the focal distances equal. The mechanical limitations to this movement meant that the best results were achieved with the smaller focal size.

3.4. Production

3.4.1 Ablation rate analysis

Production of the prototypes was subject to a series of initial investigations of different approaches. The mask that had been produced had a series of different apertures, and the purpose of these were to make a series of lines, and interface the lines in a “focus spot” made from one or more spots of different shapes overlapping each other. In order to experimentally determine the ablation rate of the samples to be produced, a series of measurements were performed. In this series, an array of lines were made perpendicular to, and across, the edge of a PMMA sample, each with a different number of points per surface area. This quantity is defined from the size of the aperture focused on the mask in combination with the shot frequency and movement speed.

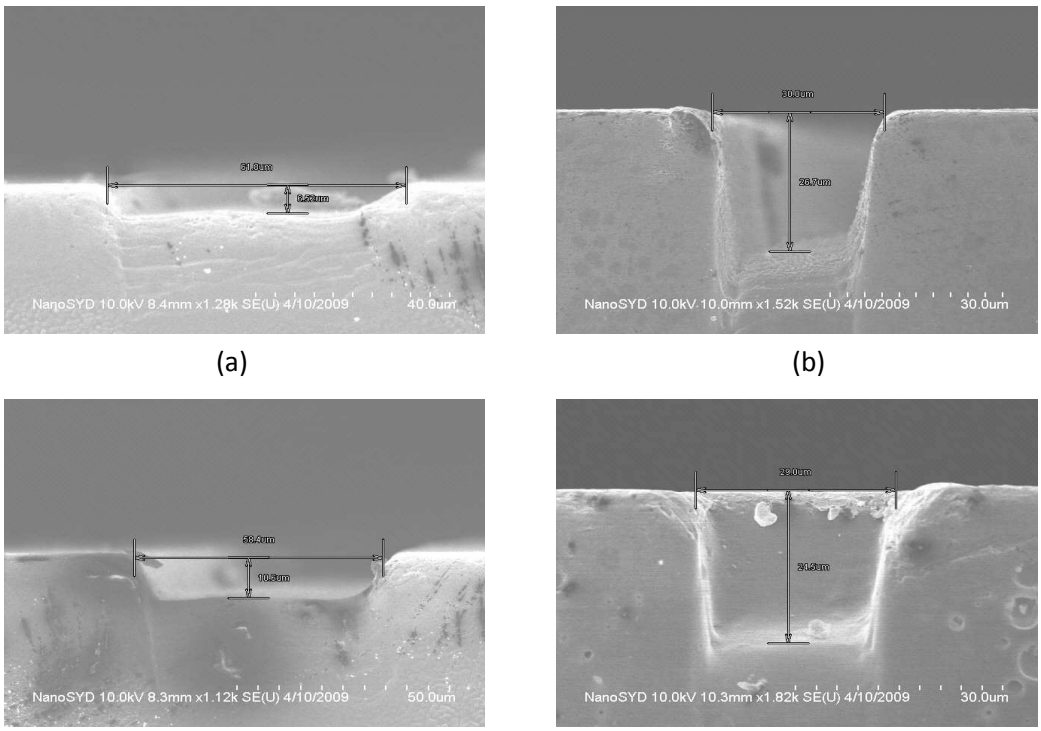

(a) (b)

(c) (d)

Figure 3-9 – SEM images used for ablation rate analysis of PMMA sample

(a) – Line shot with 60x30 µm aperture, 18 shots/area (depth: 6.52 µm)
(b) – Line shot with 30x60 µm aperture, 70 shots/area (depth: 26.70 µm)
(c) – Line shot with 60x30 µm aperture, 29 shots/area (depth: 10.60 µm)
(d) – Point overlapping line, 30x60 µm aperture, 50 shots/point (depth: 24.50 µm)

An example of the measurements performed to determine the ablation rate can be seen on Figure 3-9. In this illustration three lines are shown (a,b and c), shot with different speeds but a common shot frequency of 50 Hz. This is the highest frequency that the laser can operate with, and was chosen as standard to speed up production rate. The last image shown (d) is a hole shot with the

sample stage not moving, and the laser shooting a number of points in one position. The ablation rates of shooting either individual points one at a time or ablating a line in one process could then be compared.

When shooting individual points and intending to make a microfluidic channel, the shots have to overlap each other. An advantage of making a long line of shots all overlapping each other, is that the geometry should be uniform along the entire length of the channel, whereas a channel shot with a moving aperture will receive less fluence in the ends of the channel where the ablation is started or stopped. In order to identify which method of production that provided the best results, a number of tests were performed with different overlaps of individual points, some of which are shown on Figure 3-10.

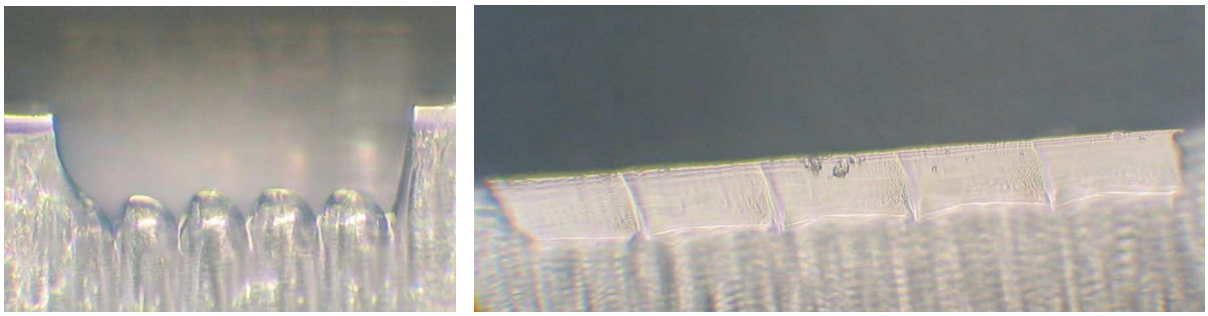

Figure 3-10 - Different overlaps of point shots were tested, to choose between stitching or line ablation

As can be clearly seen, the length of the overlaps has great influence on the bottom structure of the channel. In order to ensure a controlled flow of the fluids, as smooth a channel bottom as possible is desirable, as well as a well-defined depth. The measurements performed indicated that the channel bottom would be quite rough using the method of overlapping shots.

The challenge that would arise from instead using line ablation of the long channels in the system can be visualized on Figure 3-11, which shows the first attempt on using the mask to produce a small prototype in a polystyrene sample. The importance of aligning the apertures correctly with respect to each other can be clearly visualized, as the 4 points shot to connect the 3 input channels to the output channel on Figure 3-11.a can be seen to not actually connect the sheath flow inlets to the focus point. This is due to a small misalignment of the apertures during the manual prototyping production.

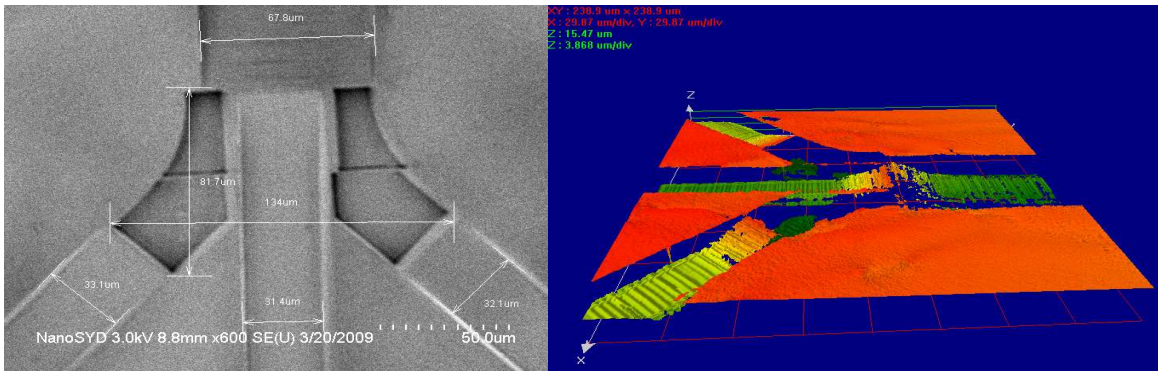

Figure 3-11 - First attempt of using mask stitching - polystyrene sample

(a) – SEM image of focus point section, showing overlapped channels

(b) – 3D representation of Interference microscope data, showing channel

On Figure 3-11.b the problem of using line ablation is visualized. As the individual line shots were all initiated from the focus point of the prototype and outwards, they all exhibit a sloping cross-section profile. At the inlets and outlet of the system this does not become a problem, but in the focus point all channels should ideally have a uniform depth all along the length of the channel. As the points connecting the sheath channels to the centre channels must be shot as points in one place, this ideal can not be achieved. The important issue is then instead to achieve as uniform a channel depth as possible, making certain not to have the system clogged by a channel not deep enough at one point.

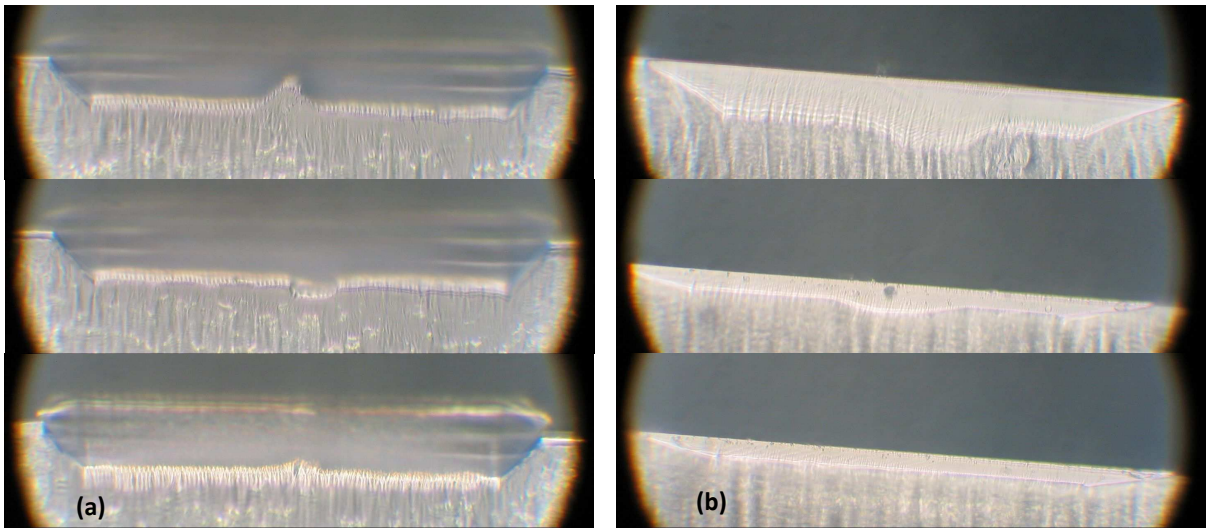

Figure 3-12 - Determining proper overlap for line ablation

(a) – Different overlaps of 30 µm wide aperture spot
(b) – Different overlaps of 60 µm wide aperture spot

In Figure 3-12 a test of different overlaps is displayed. A series of short double intersecting lines were ablated along the edge of a PMMA sample, parallel to the edge, so that the resulting image can be seen as a cross-section along the length of the channel. Two series of shots were performed with a 60x30 µm focused aperture size – one along the length (x-axis) direction of the spot, and one along

the width direction (y-axis). As the result images show, the ends of the lines shot with a 30 µm spot (Figure 3-12.a) have a slope of approximately 45° with respect to the channel bottom. In the top image the first line was started at the centre, and shot towards the left side of the image. The focused spot was then moved back to where the first line began, and an additional 15 µm (half the spot width) away from the first line. With half a spot overlapping, the ablation depth in the middle is in fact only approximately half the depth as in the rest of the channel.

In the middle image of Figure 3-12.a, the second line overlapped the first with 40 µm (the spot width + 10 µm), resulting in a little deeper groove where the overlap took place. In the lower image the second line is started the same place as the first, which should intuitively lead to the two slopes "cancelling each other out". This can be seen to be the case, albeit still with a small "bump" indicating where the overlap took place.

In Figure 3-12.b the upper and middle picture both show the resulting profile of a 60 µm spot overlapping 90 µm – one and a half times the spot size. The upper image is shot with a line speed resulting in 100 shots per area, and can also be seen to have achieved a deeper ablation than the middle image, in which 50 shots per area has been shot. In the bottom image the speed has also been 50 shots per area, and an overlap of 60 µm, or exactly the spot size. In this case it is very difficult to determine the actual overlap, as the resulting line profile appears to have a very smooth channel bottom with no sign of the overlap.

3.4.2 Prototype productions

Production of the first 2 complete system prototypes was undertaken using the determined values for ablation rate. All channels were shot as line ablations, using different apertures from the ordered mask. In the focus point a total of 4 different apertures were used to interface the channels to each other, each manually adjusted with respect to the active laser spot, and point ablation was used to remove material where the lines met.

All line end connections were designed as circle shapes with a diameter of 500 µm, incorporated into the sub-programs used to ablate the individual lines. The same apertures were used for the lines and the connections.

Production of a complete prototype was a time-demanding task. Ablation of the individual lines took between 1-3½ hours each, between each of which a new aperture should be aligned and focused to make sure that the lines would interface where it was desired. In total 2 whole days of work went into production of 2 prototypes.

Later in the process 2 extra prototypes were needed, as explained in the paragraph 3.4.4 about sealing of the systems. As there was a limited time, it was decided to change the entire process recipe into one program, ablating an entire system using the same aperture. This would of course mean a slightly different cross-section profile in the angled channels, but they were assumed to work equally well. Initial setup of the sample and laser takes approximately 1 hour, and the new

process recipe was completed in 5-6 hours, but no attention to the process in this period was required, and as such the 2 final prototypes could be produced in just one day, still leaving most of the time for other work.

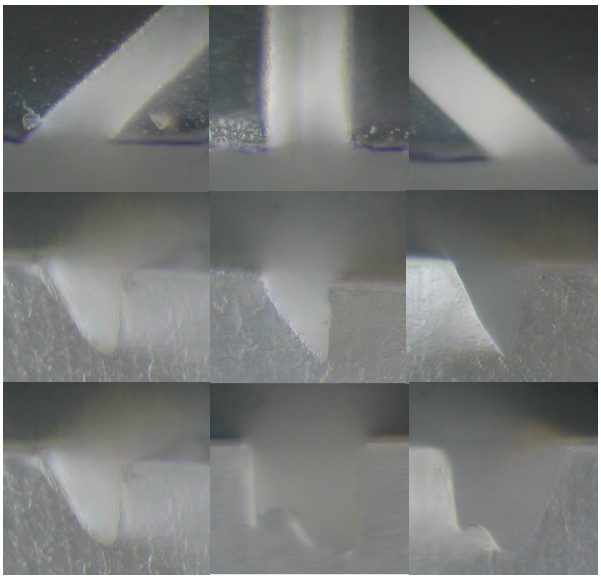

Figure 3-13 - Channel cross-section observations

In Figure 3-13 an overview of the channel cross-sections made for the 2 final prototypes is shown. The top row of images shows the angled input-channels as well as the centre input channel seen from above (ablated with the 30x60 µm aperture spot). The centre row show the channel cross-sections of prototype 3, as observed at the edge of the sample, and corresponding to the pictures above in the top row. The bottom row show the channel cross-sections from prototype 4, produced with a 30x100 µm focused aperture size.

3.4.3 Characterizing produced channels

Observing the actual depth and cross-section profiles of channels not crossing the edge of a sample has proven to be very difficult on the PMMA samples. Normal characterization technology for such a purpose would be a scanning probe microscope of some sort. The cleanroom facilities at NanoSYD offer both AFM and stylus profilometry, however the limitations regarding channel depth is highly surpassed with the desired channel dimensions. Depths of more than a few micrometres can not be measured in a channel whose width is constricted to 100 µm or less using these instruments.

An alternative to the scanning probe technologies is an interference microscope. Generating interference fringes on the surface of a sample is employed to calculate the depth of each point on the surface, and generates 3-dimensional data sets similar to those from the scanning probe microscopes. An example of an interference microscope image is the one displayed on Figure 3-11.b, which was taken from a polystyrene sample with channels less than 50 µm deep. Interference

microscopes can observe a channel from above, so it is normally not necessary to destroy the samples in order to get a cross-section profile.

Many attempts have been made to use the interference microscope in the cleanroom at NanoSYD for imaging cross-section profiles of the ablated prototypes. It has not been possible to achieve interference other than on the sample surface however, resulting in a flat profile with missing data for the entire channel area.

To be able to observe the produced channels, the laser has been used in the process of production to also ablate lines crossing the sample edges, making a cross-section profile available, observable by optical or scanning electron microscopes. This was not done during production of the first 2 prototypes however, since the interference microscope was expected to be used for providing channel cross-sections.

3.4.4 Sealing

In order to be able to perform focusing in the microfluidic systems produced, they need to be sealed. The channel structures are ablated into the surface of a PMMA microscopy slide, and this open surface must be closed to form actual channels. Due to the nature of the experiments (observing hydrodynamic focusing), the channels must be somehow observable even after sealing of the systems. In the case of the PMMA slides this is not necessarily an issue, since PMMA itself is transparent at all visible wavelengths of light. However, as most experiments in this project has been performed similarly to experiments performed in a project instead using SI slides for producing systems, a transparent seal was required. In order to be able to perform comparable measurements, as many parameters of the experiments were desired to be equal as possible – if the same method of sealing was feasible for both systems, one less difference had to be considered. Also, observation of an entirely transparent system enhances the options for observation and illumination of the experiments.

Sealing of polymeric microfluidic systems can be performed in a number of ways, as overviewed by Yussuf *et al.* in [10]. Methods researched and discussed include chemical solvent bonding techniques, adhesive bonding, different types of thermal bonding etc. In order to find a bonding method useful for both silicon and PMMA systems, it was desired to find a solution that did not involve the bulk of the sample itself as part of the bond. This objection ruled out thermal bonding methods, where typically the edge of the channels is heated using either an infrared laser shooting through the bonding material, inductive heating requiring a metallic susceptor employed in the system or direct heating of the polymer sample prior to a mechanical deformation to close the channels.

Alternative bonding methods useful for both types of systems had to be found, and the two primary methods considered would both seal the channels with a thin polyester film. One method was inspired by an online tutorial from RSC Publishing [11], in which a method of modifying a standard

office laminating machine is demonstrated. The microfluidic systems are then sealed using thin polyester films, rolled onto the surface of the system with the warm laminating rollers.

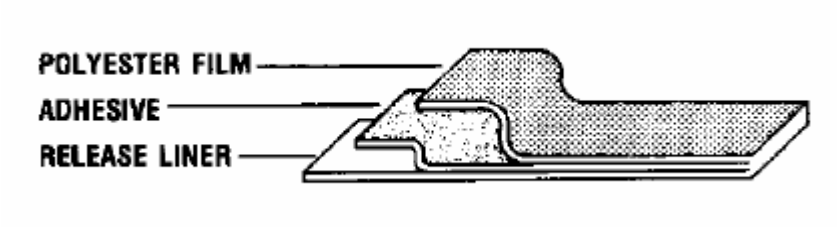

Figure 3-14 – ARcare 7815 polyester tape structure

Image source: Tape datasheet received from manufacturer on inqury[2] (Adhesives Research, Inc.)

The other method would employ a specialized tape, developed specifically for microfluidic applications. This was believed to be the sealing method which would be most intuitive to operate, and would not require specialized equipment other than what was already available in the laboratories.

A roll of tape was ordered from the supplier, Adhesives Research, Inc., and bonding of the first prototype was attempted. The structure of the tape is as shown on Figure 3-14, and application of the tape was carried out in a series of steps. First, the tape was cut to the size of the PMMA microscope slide containing the prototype system. The system was cleaned upon production in ethanol in an ultrasonic bath, followed by flushing with deionised water and finally drying with pressurized air, and was kept in a sealed container at all times in order to avoid polluting the surface. The tape and the working area was cleaned using pressurized air, so as to avoid dust and other dirt as much as possible. One end of the release liner was then carefully removed, and the tape was attached to the end of the prototype slide surface. Using a straight edge of a tool, softened slightly by application of a piece of tape around the sharp edge, the tape was subsequently applied along the length of the prototype slide, pressed in place by the tool so as to avoid air bubbles being trapped underneath the tape.

[2] Tape datasheet can be seen on appendix 3

Interfacing to the channel ends required removal of the tape just above these. A scalpel was used to remove the tape from a little area surrounding the ablated channel interfaces, resulting in these appearing as on Figure 3-15.

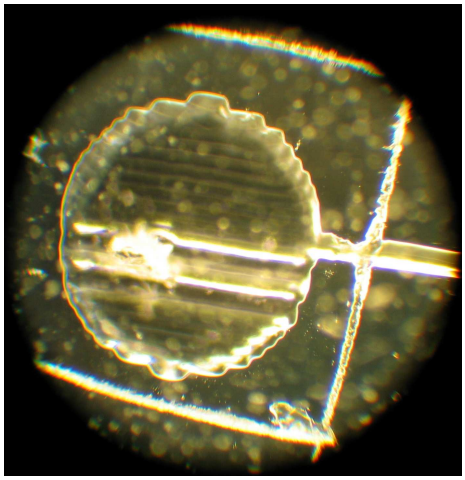

Figure 3-15 – Tape cut away around channel end connector

Interfacing to the sealed system was done using some PDMS connectors produced for the purpose – this process is described in paragraph 3.4.5. Observations of the finished prototype however revealed an error making it not likely to pump anything through the system. The channels were clogged by the adhesive on the tape, closing the channels in multiple places along their entire length. To solve this problem, it was attempted to pump water through the system, and later to pump ethanol through in order to dissolve the adhesive on the tape. Neither of the attempts was successful.

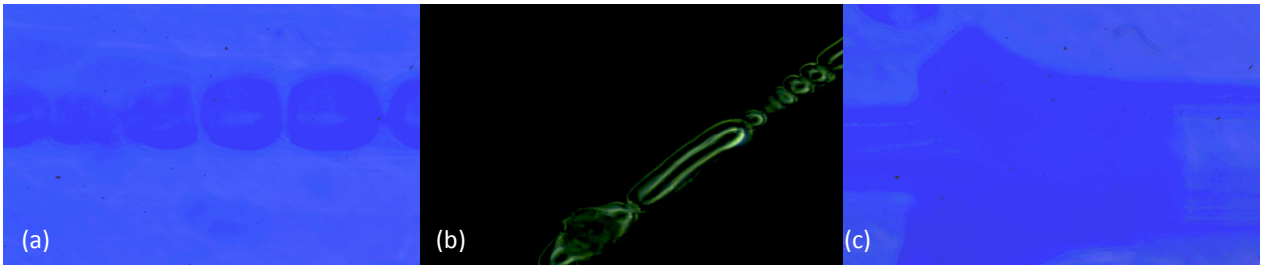

Figure 3-16 – Prototype 1, channels clogged by sealing tape

(a) – Inlet channel
(b) – Dark field image of lower sheath flow channel
(c) – Focus point – upper sheath flow and outlet channels visibly clogged

The tape could, with some care, be peeled off from the prototype again. It was cleaned once more, and attempted taped once more. It was suspected that the channel depth was smaller than expected, but due to problems with the interference microscope as explained in paragraph 3.4.3, observing the actual cross-section profile was not possible. The second attempt of applying tape was done with only minimal pressure applied along the sample surface; only just enough to ensure that no air bubbles were trapped between the tape and the channel.

A second attempt of attaching connectors to the sample inputs and output and interfacing to syringe pumps was made. As pumping water through the channels did not initially succeed, an attempt of manually applying vacuum to the output using a syringe was made, and the pumping speed slowly increased, hoping that an increased pressure would eventually result in water coming through the channels. Due to the pressure, some connectors began leaking and were exchanged. In order to seal them better, glue based on cyanoacrylate (commercially available glue, trade name “Super Attak”) was applied all around the edges of the connectors. Upon curing of the glue, the connectors began to leak instead at the top where the micro-tubing entered. Gluing the tubing to the connectors did not prove successful, as the connectors kept leaking when the pressure became high enough.

As no fluid was successfully pumped through prototype 1, sealing of prototype 2 was attempted using a different approach – lamination. A standard office laminating machine with polyester laminating pouches was used. Initial tests on some structures from previous ablation rate tests suggested that the lamination process took place at a temperature below the glass transition temperature of PMMA, not causing any harm to the structures.

Observations of the first prototype after removal of the tape used for the first sealing attempt indicated that the scalpel used to cut holes for channel interfacing had also scratched the sample surface. A possible deformation of the channel caused by this could be part of the reason why pumping fluid through the system was so difficult, and in order to avoid this, the interfacing holes were marked up on the lamination pouch and cut out before laminating.

Initial attempts of pumping fluid through prototype 2 resulted in leaking connectors, and as previously attempted new connectors were attached and glued to seal them, and the micro tubing glued in place in the connectors. Further pumping attempts upon curing of the glue resulted in the laminating sheet coming loose off of the sample surface, in turn having a large bubble of water trapped between the sample surface and the sealing sheet. Lamination using standard lamination pouches was not strong enough to withstand pressure building up, and as such was not pursued any further.

Observations on the sample after removing the lamination sheet indicated that the cyanoacrylate glue had crept down along the side of the tubing and into two of the channels. On one channel it was in a very little amount, whereas the sample inlet channel was clogged over the first 2-3 mm. of the inlet. Before attempting to remove the glue, a production of 2 extra prototypes was initiated. In an effort to decrease the flow resistance on these prototypes, channels were shortened by 10 millimetres each, both on the inlet and outlet channels.

Removal of the glue in the channels of prototype 2 was attempted by using ethanol in an ultrasonic bath, but not all could be removed. Attempts to remove the rest using a scalpel cleared one of the channels, but the inlet channel was still clogged. The excimer laser was used to ablate a new input connector in the existing channel on the other side of the glue, and the prototype was sealed again using the ARcare 7815 tape. Extensive attempts did not result in successfully pumping fluid through the prototype.

The 2 new prototypes produced were treated a little different. After laser production a white substance, believed to be particle debris from the ablation, can be observed on the surface of the

sample, especially around the ablated structures. Cleaning in ethanol in an ultrasonic bath had removed this, but for some unknown reason this had given the first prototypes a slight white discoloration on the surface at some points. As it could not be known if this process would affect the channel walls, and thus the flow, it was attempted to clean prototypes 3 and 4 differently. Compressed air was used to remove all lose particles from the surface. Lent-free optics tissues were then wetted with DI-water, and used to wipe the surface clean. Dry tissues were used to dry the surface of the sample before taping it as earlier, with the connection holes being cut in the tape before applying it.

As the cyanoacrylate glue had penetrated through the connectors on prototype 2, a higher-viscosity substance was desired for strengthening the connectors. A vulcanizing special silicone from Würth[3] was available in the laboratory, and was used around the edges of the connectors. The silicone is continuously elastic, and kept the connectors from leaking. On prototype 3, the 60 µm system, a leak appeared when attempting to raise the flow in the sample inlet channel outside of the measurement area, but a set of measurements had been performed prior to this incident.

Upon sealing prototypes 3 and 4 with tape, and sealing the edges of the connectors with silicone, 2 complete, functional prototypes were achieved and used for performing the experiments.

3.4.5 Connectors

As the prototype systems were sealed, interfaces were needed for connecting syringes to the input ports of the system and removing the fluid from the system outlet. Syringes are commonly used to pump fluids through microfluidic systems, which was also the case in this project. The syringes are mounted on a pump, and needs to be connected to the ablated microchannels. Commercial fittings for micro-tubes are available from specialized vendors, but are very expensive and not designed for prototype fabrication. An online-guide [12] was found for making connectors using a SYLGARD®184[4] PolyDiMethylSiloxane (PDMS) silicone elastomer.

Figure 3-17 - Process images from making PDMS connectors.

[3] Würth silicone datasheet is attached as appendix 4

[4] Clear silicone from Dow Corning; thermosetting two-part water- and UV-resistant product often used in electronics and solar applications for encapsulation. Data sheets and supplying information can be found on: http://www.dowcorning.com

A double-sided adhesive tape was applied to the surface of a piece of Whatman 41[5] filter paper, after which the paper was placed filter paper up in a polystyrene tray. The mixed PDMS solution was poured onto this compound, and the tray was placed on a heating plate. At a temperature of approximately 50°C the PDMS cures completely within 4 hours, and connectors can be produced.

Figure 3-18 – PDMS connector block with holes drilled for a row of connectors in the bottom

A hole is made through the PDMS/filter paper/adhesive, adequate for the micro tubing used to interface to the syringe pumps. The tubing has a diameter of approximately 1 mm. As the PDMS silicone is elastic also upon curing, the holes through the connectors were made with an Ø0.8 mm. drill, securing a tight fit in the connectors. A scalpel is used to cut the connectors out of the block (Figure 3-18), and as such they can be made to have the desired size. In order to avoid leaks, a large tape surface area on the underside is desired, without blocking observation of the system.

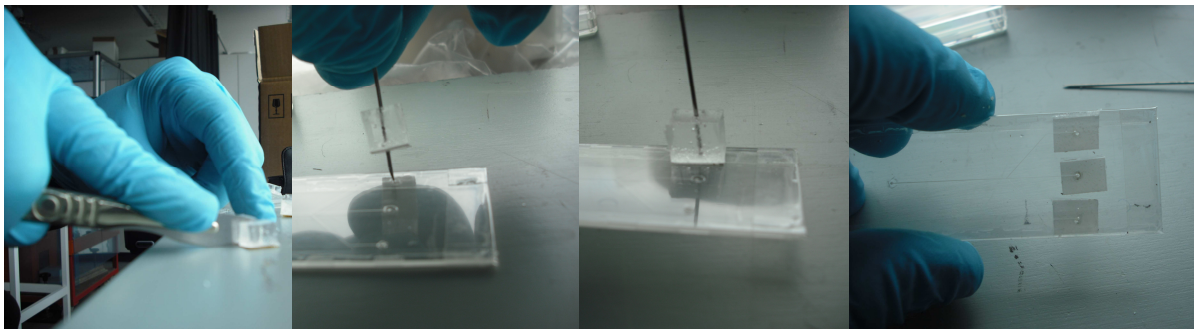

Figure 3-19 – Illustration of the connector mounting process

Mounting the connectors is done using a syringe needle for removing debris from the drilling operation and aligning the hole for the micro tubing with the holes in the tape covering the sample. The process of cutting and mounting connectors is illustrated on Figure 3-19.

[5]Whatman 41 is a standard, Ashless filter paper for laboratory uses. More information can be found on: http://www.whatman.com/QuantitativeFilterPapersAshlessGrades.aspx

3.5. Performing experiments

The prototypes made in PMMA for this project and those made in silicon in the parallel project both exhibit outer dimensions bordering on the limitations of the human eye. Because of this, magnification and fine control of delicate motion along 3 axes are vital for success in observing and quantifying the achieved focusing.

Casper Kunstmann-Olesen, Ph.D. student employed in the Lab-on-a-chip project, is developing a test platform for the measurements and analysis in this project. As the optics company Navitar Inc. has supplied most of the optical components on the test platform, it goes by their name in the laboratory. An initial version of this "Navitar" test setup was used for performing measurements on the prototypes, and some tests were made on the silicon systems. As the setup (depicted on Figure 3-20) is still under development, it was in a state where measurement quality was greatly affected by mechanical vibrations and background noise from the laboratory environment. Likewise, the light source for the samples was coupled in a way that could not ensure uniform illumination all across the width of the microchannels.

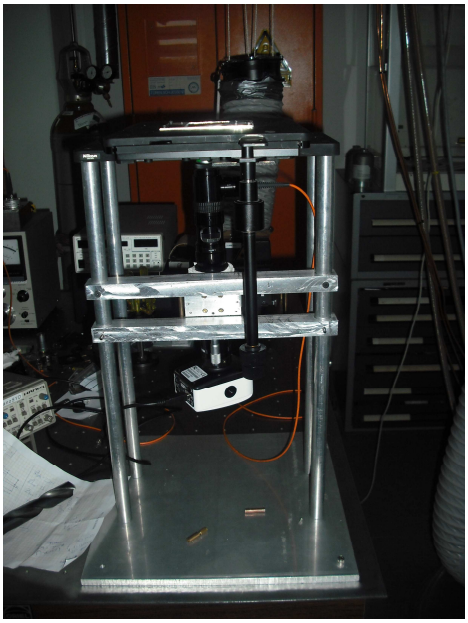

Figure 3-20 – "Navitar" experimental setup

All experiments in the project have been performed using a fluorescent fluid (DI water colored with Trypan blue[6]) through either the sample or the sheath inlets. The main motivation behind this is having comparable results across different prototypes and systems. The commercial system as well

[6] Trypan blue is a colorant designed for viable cell counts of mammalian cells in experimental biology. Only cells that are non-viable (not fit for survival) will accept staining when subjected to the colorant. Upon illumination with UV light the colorant exhibits fluorescence.

Source: Product information sheet, Stemcell technologies Inc. Attached as Appendix 5.

as the PMMA prototypes made in this project are both transparent in the visible range of light, so experiments with light from one side of the sample and observation from the other could have been performed on these systems, but this would not be feasible in the silicon prototypes that the results should be compared to.

As the test setup was not yet in a state where reliable images could be acquired, a different setup had to be used. A Nikon optical microscope equipped for fluorescence microscopy was used. Both the commercial focusing system and the PMMA samples were the size of standard microscope slides (25,5x75,5 mm), the microscopes sample holder could be used directly. The silicon systems could be mounted on top of a glass slide to fit on the sample holder.

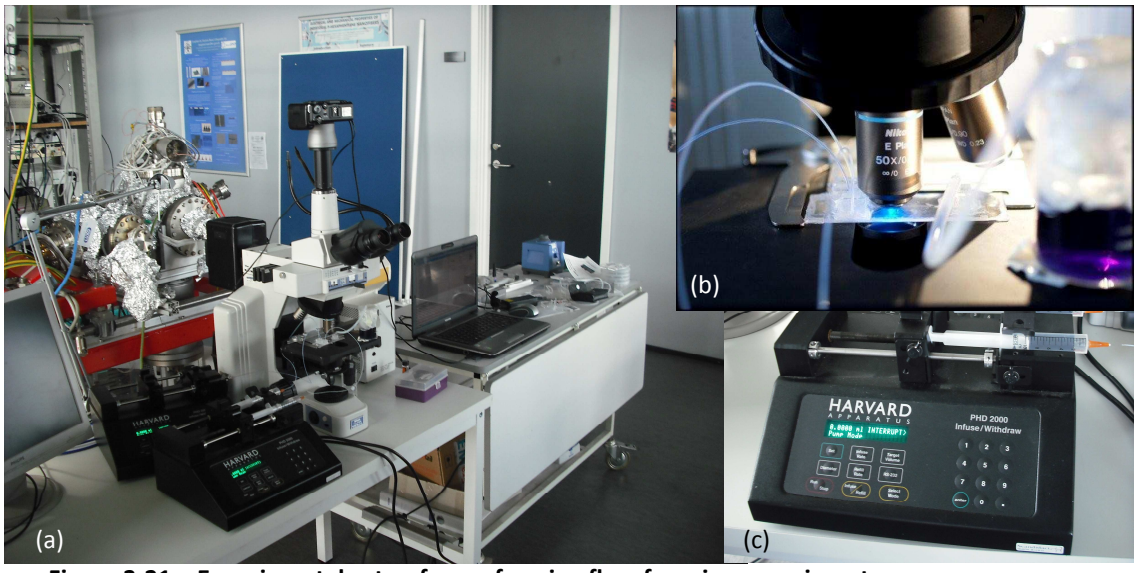

Figure 3-21 – Experimental setup for performing flow focusing experiments

(a) – Overview of setup with pumps, microscope, camera and computer
(b) – Close-up image of prototype during testing (courtesy of photographer K. Riggelsen)
(c) – Harvard PHD 2000 syringe pump driving sheath flow channel syringes

Figure 3-21 shows the experimental setup used. The fluid was administered using Harvard PHD 2000[7] syringe pumps and standard 10 ml. disposable syringes for the sheath flows. The sample inlet flow was administered using a Hamilton Gastight[8] 50 µL syringe on a second syringe pump. The pumps were manually controlled, and results were documented using a Canon Powershot G5 digital camera mounted on the microscope and connected to a computer. All measurement flow settings were performed according to the experiment setup model described in paragraph 2.5.

[7] Users manual for the pump with specifications can be found on: http://www.instechlabs.com/Support/manuals/PHD2000manual.pdf

[8] Glass syringe for high precision fluid administration. Data sheet and further information is attached as Appendix 6.

3.6. *Flow measurement analysis*

Measurements of the width of the focused flow in the channels have been performed using the program SPIP (Scanning Probe Image Processor). This software is intended for treating datasets acquired through scanning probe microscopy, but holds some features which make it useful for analysis of images from the fluorescence microscope as well.

In order to determine the image resolution (in pixels/µm), some images of a structure with known dimensions were first acquired, using the same microscope objective as when performing the actual measurements. These images were then analysed in the program, and the resulting scaling factor could be applied during consecutive measurement analysis.

The program SPIP treats the microscopy images as a three-dimensional dataset, with the color of the individual pixels as the height information (z) of that particular coordinate. In order to measure the width of a focused stream of fluorescent fluid, a high contrast, sharp image necessarily provides the best results.

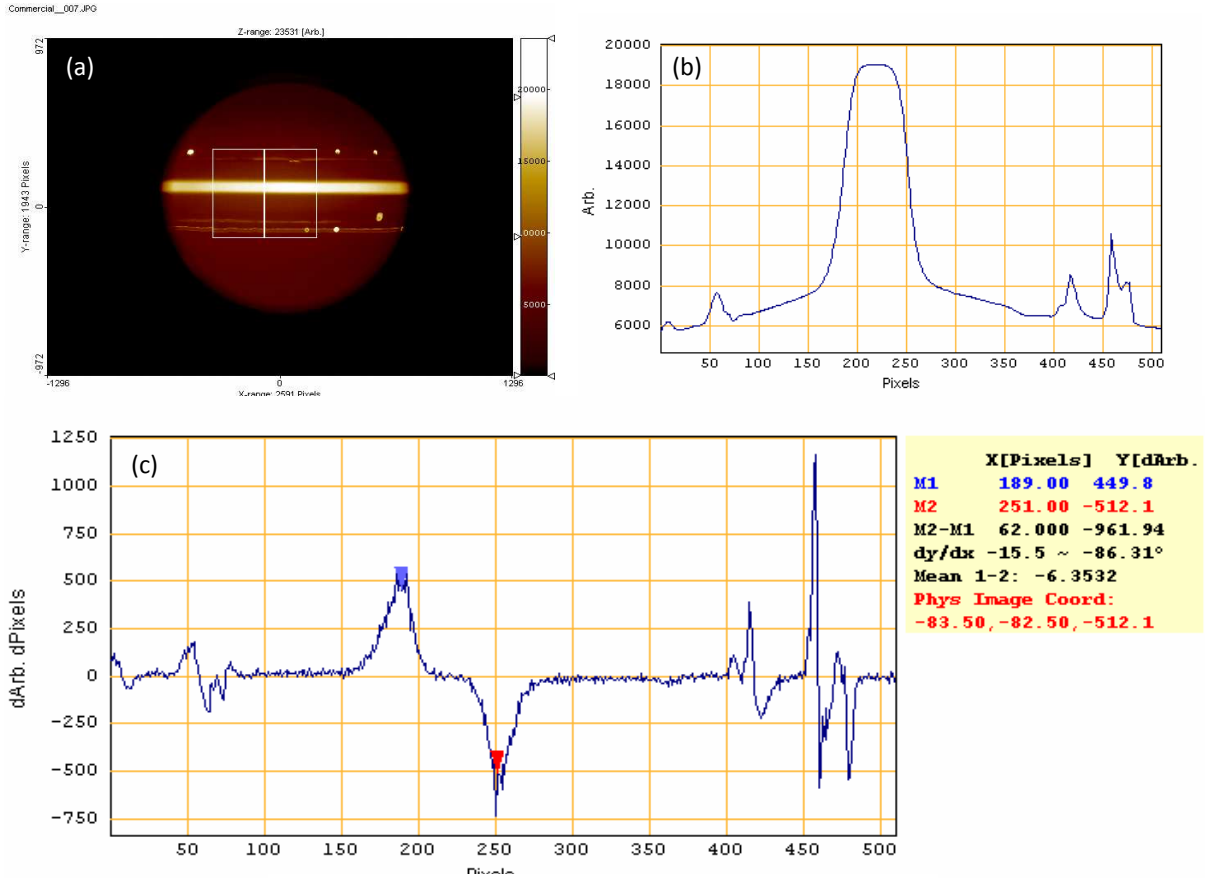

Figure 3-22 - Data processing in SPIP

(a) – Microscope image with averaging line
(b) – Averaged cross-section profile
(c) – Profile gradient image with measurement cursors

To find the width of the focused fluid, an averaging line profile was applied across the image of the focused beam (Figure 3-22.a). The resulting profile (Figure 3-22.b) exhibits an obvious peak, analogue to the intensity of the fluorescent light from the focused flow. Due to diffraction of the fluorescent light, the edges of the flow profile does not stand out very sharp. In order to determine the width, the gradient of the averaged profile was used for analysis instead, inspired by [15]. This gradient image (Figure 3-22.c), makes it possible to find the turning-point of the profile edge, and the distance between the two turning points is directly proportional to the width of the focused stream, w_f.

However, due to a "noisy" gradient profile it was found difficult to determine the exact turning-points of the profile in many cases. In order to ensure proper comparison of different data, a method was investigated to smoothen these profiles, giving a more well-defined measurement point. SPIP can apply different filters to the data, and a meaning filter was selected, with an averaging length of 11 pixels, as can be seen on Figure 3-23.

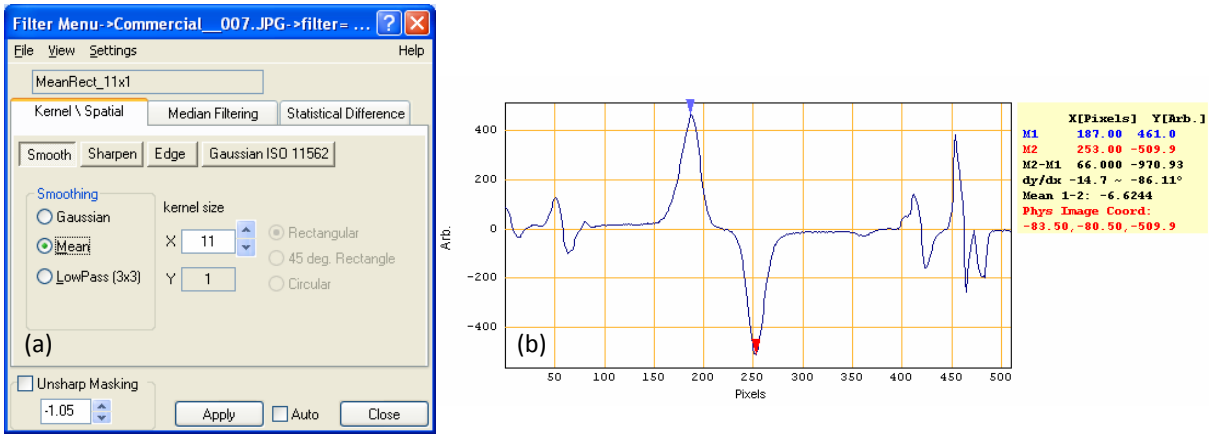

Figure 3-23 – Filter settings for smoothing of gradient profiles and resulting channel gradient cross-section.

(a) – Filter settings. In this case the filter was set to perform simple averaging over an 11 pixel wide area.

(b) – Channel cross-section after meaning, corresponding to that of Figure 3-22

The settings of the filter were determined through a series of tests with different filter values. A meaning filter was selected as the purpose of filtering was simply to smoothen an uneven curve. Visually the curve became more and more smooth with increasing filter kernel size, yet too high a value would result in rounded peaks, complicating precise identification of the curves' turning-points.

A test sample with a series of parallel metal lines on the surface was used to calculate the conversion factor between images taken with the camera on the fluorescence microscope in pixels and the actual dimensions of the lines (which were known) in µm. All focusing tests on the commercially available microchannel system as well as the prototypes produced in the two projects were made using the same fluorescence microscope, with a 50x objective to observe the channels. The test sample had a number of parallel lines, known to be exactly 35 µm wide and spaced 15 µm apart. Measuring from one edge of one of the channels to the same edge on the second channel from it would give a precise measurement of 100 µm.

Figure 3-24.a shows a sample image being processed in SPIP. An averaging profile line is made to cover 3 lines next to each other, as shown on Figure 3-24.b. Each line has a peak at both sides of the line, so a total of 6 peaks are seen in this image. A number of measurements were performed directly on this averaging profile, as it had very nice peaks for placing the measurement cursors. In Figure 3-25 a chart is shown containing a series of measurements used to determine what kernel size would give the most uniform results when applied to a series of images. The measurements from the averaging profile is shown in the lower right corner of the chart, and 3 consecutive measurements show an average scaling factor of 371,6667 pixels/100 µm, or 3,717 pixels/µm.

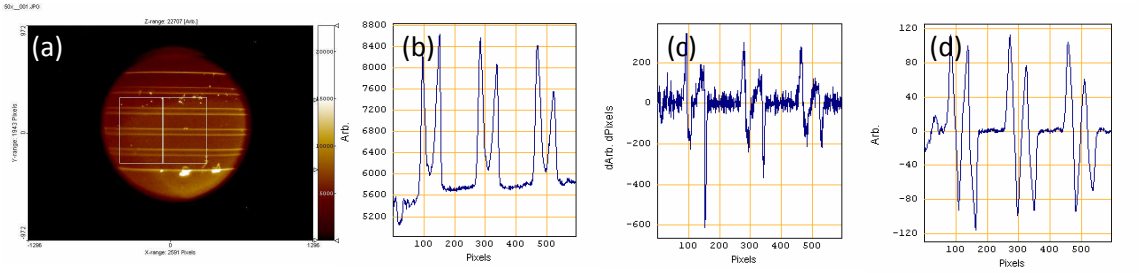

Figure 3-24 – Examples of test-graphs for different filter kernel size values

(a) – Raw image of test sample showing 3 lines, 35 µm wide and 15 µm apart

(b) – Averaged cross-section profile across lines, as indicated by white rectangle on (a)

(c) – Gradient image (dy/dx) of cross-section profile (b), used to measure distances

(d) – Smoothened gradient image (dy/dx) after meaning filter with 25 pixel kernel size

Analysis of the experimental data was in all cases performed on the gradients of the cross-section profiles, as most images had a less sharp defined overlap between the focused stream and the sheath flow. Taking the derivative of the profiles would result in peaks on the turning points of the cross-section profiles, which is then regarded as the edge of the focused stream of fluid. A number of measurements were performed on the gradient images before applying any filters, and some of these results are shown in the upper right-hand corner of the graph on Figure 3-23 – giving an average scaling factor of 3,732 pixels/µm.

Kernel size	Filter applied to dy/dx graph			Filter applied to raw image			dy/dx graph without filter applied		
	Upper	Lower	Avg.	Upper	Lower	Avg.	Upper	Lower	Avg.
3	372	376	374	372	375	373,5	371	374	372,5
5	372	375	373,5	371	376	373,5	372	374	373
7	373	374	373,5	373	374	373,5	372	376	374
9	372	373	372,5	372	373	372,5			**373,1667**
11	372	372	372	372	372	372			
13	374	371	372,5	374	371	372,5	Meas. on avg. cross-section		
15	373	371	372	373	372	372,5	Upper	Lower	Avg.
25	372	371	371,5	373	371	372	372	371	371,5
35	373	371	372	374	370	372	372	371	371,5
55	373	368	370,5	372	371	371,5	373	371	372
			372,4			**372,55**			**371,6667**

Figure 3-25 - Chart used for filter kernel size determination

The columns on the left side of the chart shows the measured values for a 100 µm known length, with filters of different sizes applied either to the raw data of the image before averaging across the lines or applying the filter to the gradient profile directly. The best result was expected to be that in which the filter is not employed until the derivative formula has been isolated. Small rounding errors in a formula can end up changing the end result a lot, so the later in the process the smoothing takes place, the less distortion of the results should take place due to the filtering.

As the graph shows, a column of different kernel values for the meaning filter has been tested, both for applying the filter to the raw image data and by applying it to the gradient graph instead. The smaller values would tend to not smoothen the graphs enough, so there would still be doubts about where to place the cursors for reading out the width data. Large values for the filter would instead result in a profile so smooth that the turning points were no longer easily identifiable. A good value was determined to be between 7 and 13, since different experiment results tested with these values were all easy to measure. In the end the value 11 was selected, as all measurements performed with a filter having a kernel size of 11 gave the exact same result, regardless of whether the filter was applied to the raw image data or to the gradient profile.

The pixel to µm conversion factor was set to 3,724 pixels/µm, as the average measured values indicated. It was decided to perform two sets of measurements on the experimental data – one on the un-filtered gradient profile, and one on the gradient profile after applying the smoothing filter. These results could then be compared, to indicate whether the measured values correspond to the estimated flow focusing.

4. Results

4.1. Ablation rate determination

The amount of material ablated due to a certain number of shots with the laser was determined experimentally, in order to be able to write programs for controlling the ablation of the prototypes. These measurements were made on a purchased PMMA sample, having a very smooth surface, and also very nice side edges due to their production (by injection moulding). The cross-sectional profile of the ablated points/channels was what was desired to observe. For structures with smaller depths a scanning-probe microscopy method could have been employed, however the achieved structures were expected to have, and had, dimensions rendering these methods useless for determining the ablation rate.

Proper observations with an interference microscope also proved to be extremely difficult to achieve on the ablated structures. Early ablation rate experiments in the project were made using the excimer laser to cut a deep groove in a sample, and shooting points or lines perpendicular to this groove. This enabled later mechanically cutting through the remainder of the sample thickness, and getting a very well-defined edge structure, in which the ablated channels could be observed using either an optical microscope or a SEM following deposition of a thin layer of gold on the surface.

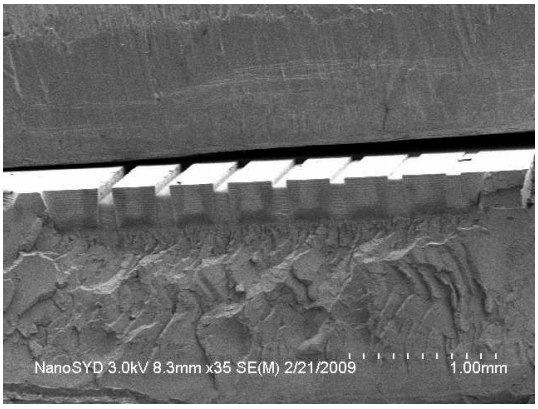

Figure 4-1 - Overview of initial ablation rate determination – Polystyrene sample

Figure 4-1 shows one of the early experiments, performed on a polystyrene sample, and observed in a SEM. Detailed images such as those that can be seen on Figure 4-2 could be used to directly measure achieved ablation, and as such determine the ablation rate from a series of measurements.

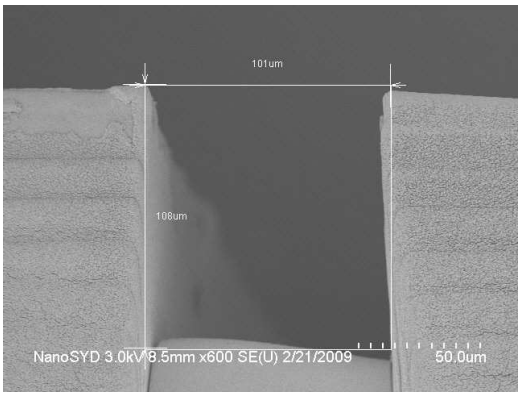

Figure 4-2 - Close-up image of channel with dimensions, used for determining polystyrene ablation rate

Initial experiments were performed on PMMA samples using the same method – ablating a deep trench, and ablating lines or points perpendicular to this trench. It was found very difficult later on to break the PMMA samples in order to observe them.

The polystyrene samples initially tested were small – approximately 12x24 mm, with a thickness of 2.5 mm. Upon ablating a groove of approximately 500 µm depth, there was still enough material to enable cutting from the other side of the sample with a circular saw blade, as indicated on Figure 4-3.a, without risk of cutting into the groove thereby destroying the fine structures to be observed.

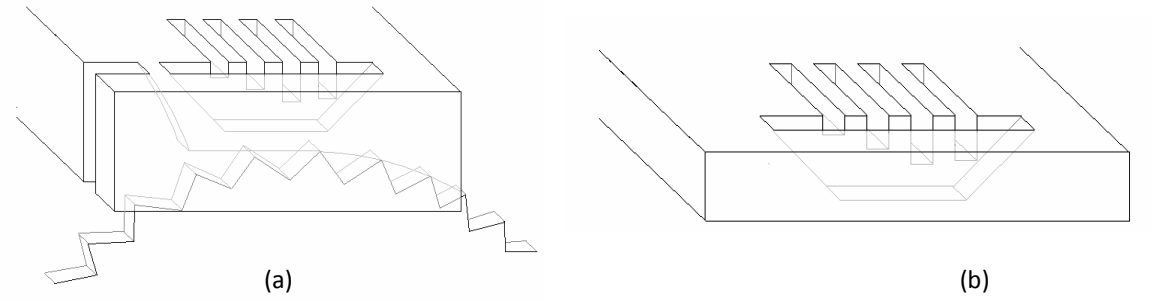

Figure 4-3 – Cutting of ablation rate sample

(a) – Method used for thick polystyrene sample

(b) – Problematic PMMA sample too thin for sawblade

…

The PMMA samples acquired for the project has a thickness of only 1 mm. Due to the heat developed when using the circular saw blade for cutting through the samples, and the nature of the polymeric material, great deformations take place where the saw blade touches the sample. This complicated breaking the PMMA samples in which the ablation had been made, as the saw blade could not be controlled precisely enough to make sure that the ablated channels were not destroyed. The first attempts of breaking the PMMA samples were made with the circular saw blade, in turn destroying the sample. New samples were produced, a rather time-consuming task, and an attempt was made to scratch the samples using a scalpel blade, before mechanically breaking them.

The PMMA samples showed more brittle tendencies than the polystyrene samples, and did not break exactly at the ablated grove, once again rendering the fabricated sample useless.

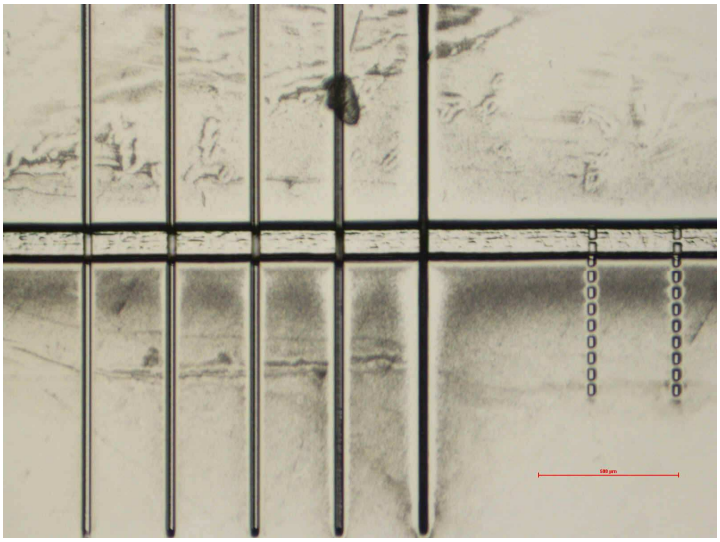

Figure 4-4 – Overview of the PMMA ablation rate sample, before attempting to break it for observation

The process of fabricating ablation rate determination samples was altered, leaving out the initial fabrication of a deep groove, instead using the edge of the PMMA sample directly, ablating lines and points across this edge. The polystyrene samples were cut down to size, resulting in rough edges, but as the PMMA samples were injection moulded the edge was smooth enough to be used directly for ablation rate analysis.

Observations of the initial polystyrene sample tests were performed using a SEM, and those made of the later PMMA samples were performed using an optical microscope. A series of calibration images were taken of a sample with known dimensions, and these images were used to calibrate image processing software for subsequent measurements.

4.1.1 Point ablation

Ablating lines by shooting a series of pulses at one coordinate before moving the sample, letting the individual points overlap only a fraction of the total spot width was one strategy that was investigated. For this application, a series of shots were made, 2 of each, with an increasing number of shots per point. The resulting ablation rates were measured and the relation between number of shots and achieved ablation rate determined.

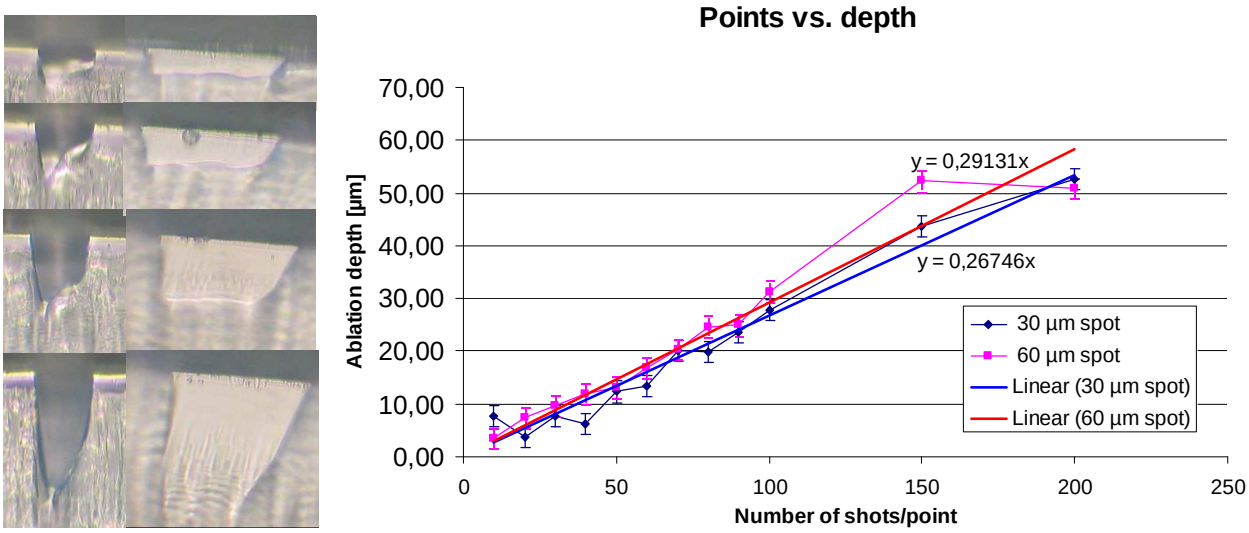

Figure 4-5 - Images and graph of individual point ablations

As the graph on Figure 4-5 indicates, two series of tests were performed – with two different spot sizes. The two tests were in fact performed using the same aperture, with a 30x60 µm focused size, each test along one of the axes of the aperture. The purpose of this was to determine whether the fluence along the entire width of the aperture could be regarded as equal along both axes, or the focusing objective would distort it. The results showed fairly nice ablation results, however less well-defined shot cross-sections as with the earlier polystyrene samples. The bottom of the shots became less flat with increasing depth, suggesting that deeper ablation should be performed whilst varying the focal distance of the sample to achieve the best results. In practice this could be performed by ablating a smaller depth in one shot, moving the focus according to the ablated depth, and continuing the ablation.

The ablation rates of the two series were rather close. Measurement errors were estimated by performing a number of repeated measurements of the same images, and noting the difference between the individual measurements.

4.1.2 Stitching line bottom

When using point ablation to create lines, the individual points are overlapped more or less. Ideally the aperture would result in a very well-defined, rectangular spot being shot on each point. In practice, the edges are not always aligned 100% to the axes of the stage moving the sample, as even very small angular displacements can affect the result. This fact makes precise adjustment of the individual shots with respect to the neighbouring shots difficult without having a small overlap of the shots. The area which is overlapped will be subject to similar shots twice. A series of tests was performed, again along both edges of a 30x60 µm spot size, and the measurements were used to determine the average ablation rate along the channel.

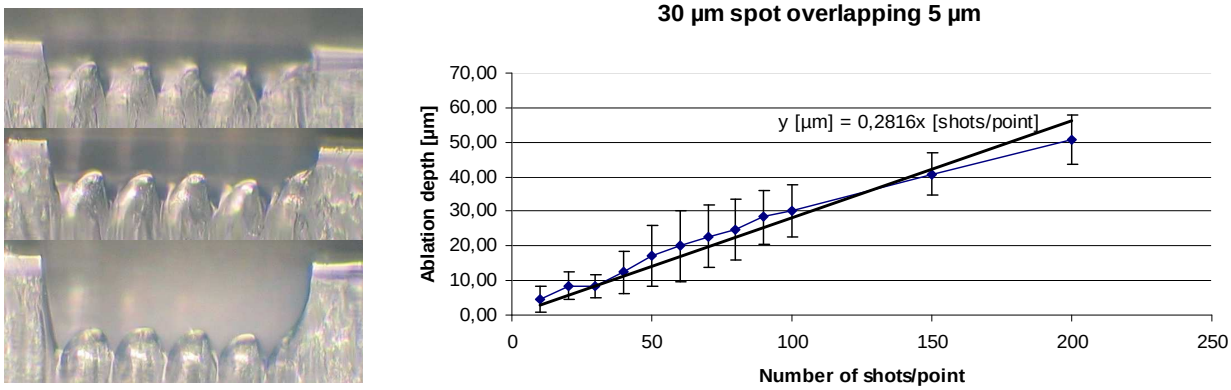

Figure 4-6 - Point overlap test pictures and graph - 30 µm spot, 5 µm overlap

As indicated by the graph on Figure 4-6, the ablation rate measured is rather close to that of the individual shots. The measurement errors indicated are quite a lot larger, which is due to the interpretation of the image data. Sample images clearly show the difference between the depths where the points have overlapped and where they have not, and two depths were measured for each image. The depth of the overlap “trenches” and the depth of the “tops” between them have been used to calculate an average ablation depth for the channel (not considering the length of the overlap, merely a meaning of the two measured depths). The difference between this average ablation depth and the depth of the trenches, equal to the difference to the tops, has been added as measurement errors on top of the ones due to measurement inaccuracy.

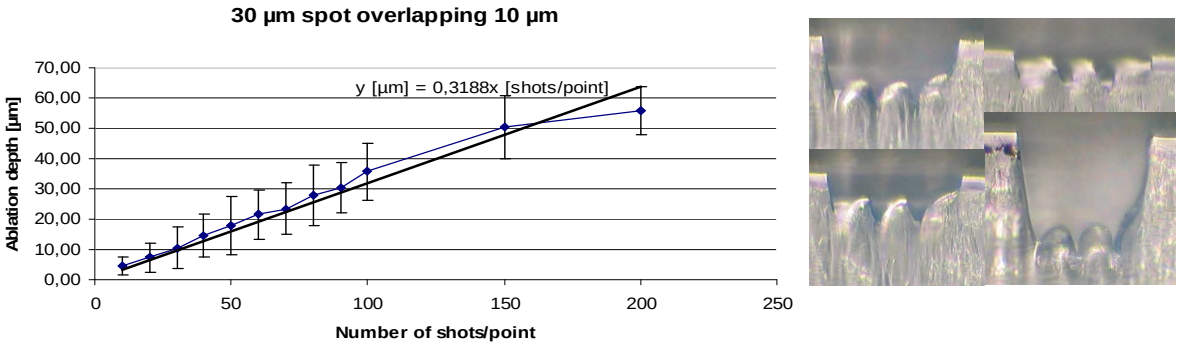

Figure 4-7 - Point overlap test pictures and graph - 30 µm spot, 10 µm overlap

On Figure 4-7, the spot width is still 30 µm, but the overlap between individual shots has been increased to 10 µm. This would be expected to result in an ablation rate close to the previous one, perhaps a little higher, which the results confirm. In the centre of the overlap "trenches", they become a little deeper than those with the smaller overlap, resulting in a mean ablation rate a little bit higher.

When similar tests were performed perpendicular to the others to give a 60 µm spot width, results were looking nicer. This might in part be due to a real spot size of slightly less than 60 µm, resulting in a shorter overlap width than the intended 5 µm. There are still clear indications on the channel bottoms of the individual points, resulting in quite rough channel bottoms, but the resulting channels are much smoother than those performed with the 30 µm spot width, as the images on Figure 4-8 also indicates.

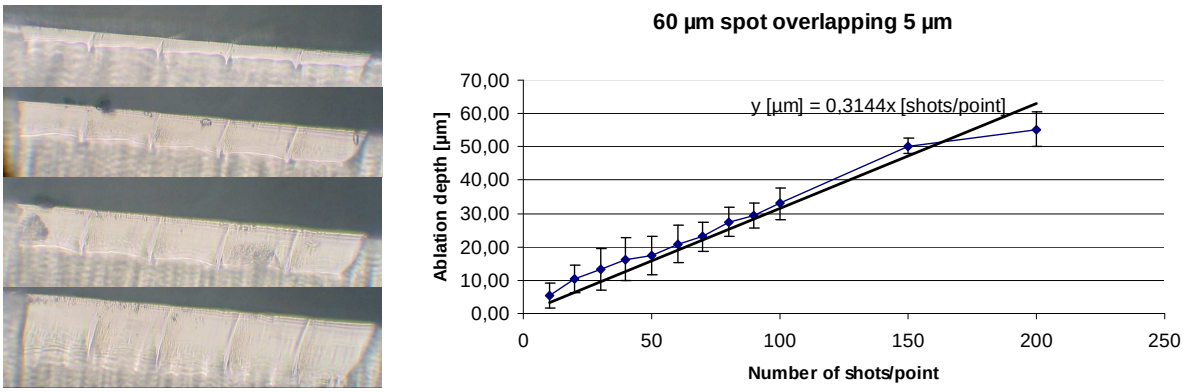

Figure 4-8 - Point overlap test pictures and graph - 60 µm spot, 5 µm overlap

When generally considering point-by-point stitching of lines rather than line ablations with a constantly moving sample, the main advantage is a uniform channel depth even at the ends of the channels. Due to the large amount of information necessary to ablate each point in the right position the program files for controlling this type of ablation tend to be much larger than those used for line ablation, in turn resulting in slower production speeds.

4.1.3 Line shooting

As the excimer laser used can only operate as a pulsed laser, the term line ablation can in fact be a bit misleading. Principally the same thing happens as with point stitching – a series of pulses hit each place that should be processed, resulting in an ablation taking place. The main difference is that in line operations, the sample is moved between individual pulses of the laser, and the overlap between consecutive shots is typically many times higher than that of the "point stitching" method. In principle it would be possible to write a program that did the exact same thing, by shooting only a single pulse with the laser, moving the sample a very short distance before shooting another pulse etc. This method is limited by the smallest distance with which the sample stage can be moved, whereas for line ablation the pulses may be fired in the midst of the movement.

In order to be able to compare the ablation rates achieved with point stitching versus line ablation, the number of pulses that the line is subjected to per length should be the same as those measured in point ablation. This number is calculated by the following formula:

$$\frac{\text{shots}}{\text{length}} = \frac{\text{spot width}\,[\mu\text{m}] \cdot \text{shot frequency}\ [\text{pulses/s}]}{\text{movement speed}\ [\mu\text{m/s}]} \qquad \textbf{(4-1)}$$

In order to make production of the ablation rate samples (and subsequently of the prototypes) as fast as possible, the frequency of the laser pulses has been kept constant on 50 Hz, the highest speed with which the laser setup can continuously operate without overheating. As the spot size is also constant throughout ablation of a line, the number of shots per length varies inversely proportional to the movement speed of the sample stage.

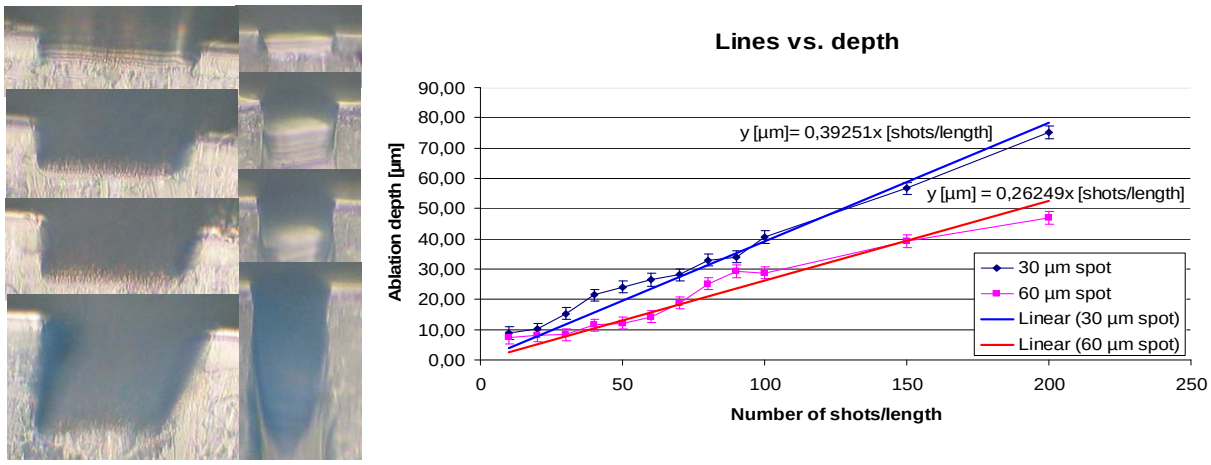

Figure 4-9 - Images and graph of line ablation

As the graph on Figure 4-9 indicates, the ablation rate was a little higher when ablation took place along the 30 µm spot – producing 60 µm wide channels due to the 30x60 µm side lengths of the spot. The bottom of the channels also appeared from the cross-section images to be more flat. In general the surface quality of channels ablated using “line ablation” is much greater than that using “point stitching”. The disadvantage of this method appears most clearly when channels should meet and intersect, as the channel ends slope due to starting or ending of ablation, requiring more careful production.

4.1.4 Ablation rate conclusion

The different investigations have revealed the strengths and weaknesses for using both individual point stitching and ablation. In the production scheme for the prototypes, a combination of the two was desired, using line ablation for the long lines and end connectors, and point stitching for interfacing the channels at the focus point. In practice this was a very time-consuming method, resulting in no fully functioning systems, so the final prototypes was made using only a single aperture working only in line ablation.

(Ablation)/(Shots/area)	30 µm spot	60 µm spot
Point ablation	0,26746	0,29131
Point 5 µm overlap	0,2816	0,3144
Point 10 µm overlap	0,3188	N/A
Line ablation	0,39251	0,26249
Average value	0,3150925	0,2894

Figure 4-10 - PMMA ablation rate chart

The trendlines added to the ablation rate plots in this section all have gradients between 0,26 and 0,39, for both point ablation and line ablation. This basically relates the number of individual laser pulses to hit a certain area of the sample surface to the ablation depth of material from that same area. The gradients of these trendlines have been compared in the chart in Figure 4-10, and the average values for ablation using either a 30 or a 60 µm spot are very close to each other. This should be the case, as all tests were performed using the same aperture, adjusted once, and the tests were performed along the x- and y-axes of the sample stage.

As the average for the two spot sizes are on either side of the value 0,30, this value has been used to approximate the ablation rate when preparing programs for production of the prototype systems.

4.2. Focusing experiments

The two prototypes, prototype 3 and 4, which were successfully sealed, were used to perform the experiments described in this section along with a 100x100 µm silicon system produced by Bjarke Jacobsen. Prototype 3, made with a 30x60 µm spot to have an approximated channel cross-section of 60x60 µm, is described in this section as “60 µm PMMA system”. Prototype 4, made with a 30x100 µm spot for a cross-section of 100x100 µm is described as “100 µm PMMA system”.

Performances of the different focusing systems have been plotted as a function of the simple model used to estimate the width of the focused stream. A series of result plots have been produced, in which the expected focus width in percentage of the output channel width, as function of the ratio between the sample input flow and the total output flow, is plotted as a solid, blue line.

For all systems the expected and achieved focus width has been plotted as percentage of the output channel width, making the plots directly comparable in spite of different output channel widths.

In all plots 2 sets of data has been shown. As previously discussed, the experimental data has been measured both with and without a filtering to ease the correct placement of measurement cursors in the image processing software. The data acquired from positioning the cursors as accurately as possible without filtering the gradient curve is labelled “Measurement data” on the subsequent result plots. On the same plots results achieved after filtering the gradient curve are also displayed, so the possible difference between the two measurement forms can be observed. These results are labelled “Smoothened results”.

Measurement errors occur mainly from misplacement of cursors on the gradient curves in the image processing software. As the cursors are manually placed, and the curves on which to place them in many cases are very rough, the exact positioning of the cursor can vary from time to time. In order to minimize errors, the same person has performed all image analysis on a given system, and done it in one sitting. To determine the accuracy of the analysis, the same person has redone a selection of the measurements on the given system after a few days. The largest difference between two measurement results on the same image is then considered the highest possible attainable measurement error for that particular system – on either side of the data value. The measurement error is considered to be an extreme case of “misjudgement” with respect to the first measurement, and an equally large misjudgement could have possibly happened “to the other side”.

The largest measurement deviation on the control images is regarded the maximum error for the particular system as a whole, and error bars are added to the plot correspondingly.

On the following pages the different channel systems are displayed and discussed.

4.2.1 Commercial system

Initial tests were performed on the commercial system acquired for the project. Familiarizing with the test equipment and practical setup of the test was investigated on this system early in the project phase, and the measurement process was developed using this system.

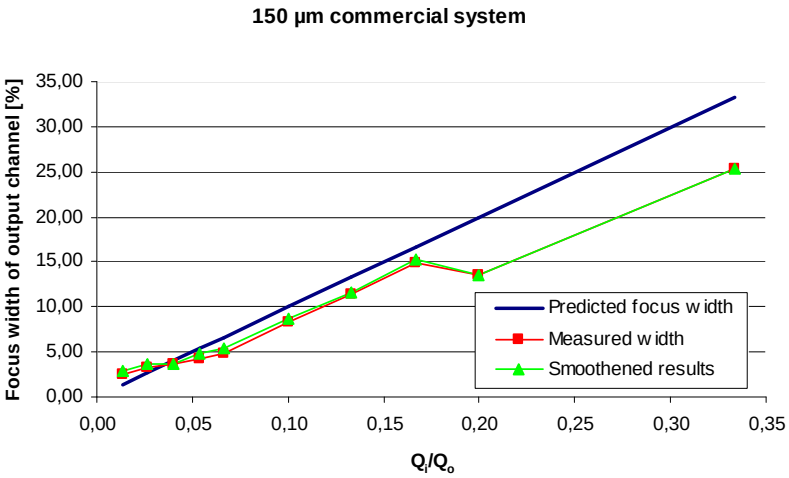

Figure 4-11 – Flow measurements on commercial system

As the plot title on Figure 4-11 indicates, the output channel of the commercial system is 150 µm wide by 100 µm deep according to the datasheet from the supplier. Based on the simple theoretical predictions the focused flow width should follow a straight line as indicated by the blue line on the plot above. The quality of the experimental images from this system were some of the best images achieved – the borders between the focused flow channel and the sheath flows were sharp, and image analysis could be performed quickly.

Since the errors between two different image analysis sessions were virtually non-existent (highest error was 0,18% off of the earlier measurements), no error-bars have been included on this graph. The sharpness of the images is also visible by the fact that results with and without filtering are almost completely identical.

On the commercial system focusing down to a width of approximately 2,5 % of the channel can be controlled – on this system that means that the actual width of the focused channel can go down to approximately 3,75 µm. Focus sizes above approximately 15% of the output channel width, or 22,5 µm, does no longer follow the line of the predicted focus, but as this is far above the size range it is interesting to be able to control, it is not really that big an issue.

4.2.2 60 µm PMMA system

The 60x60 µm channel system, produced in one ablation process with a 30x60 µm aperture size, was the first PMMA system in which water was successfully pumped through all 3 inlets and let out through the outlet channel on the other end of the system. As the focus widths that were attempted to achieve on all tested systems ranged from 2 to 30 µm, plus a final width of ⅓ of the output channels width, the number of measurements to be performed on this system was lower than that of systems with wider output channels. Specifically, the 7th measurement out of 10 was a focus width of 20 µm, which in this system is equal to ⅓ of the output channel – so the remaining 3 measurements should not be performed.

Initially the plan was to perform the seven measurements, and then repeat them with inverse coloring – fluorescent colored fluid in the sheath flow channels and ordinary DI-water in the centre channel. It happened to be so that the input connectors to interface the micro-tubing to the system began leaking just after performing the seven initial measurements, so the inverse test could not be performed on this system.

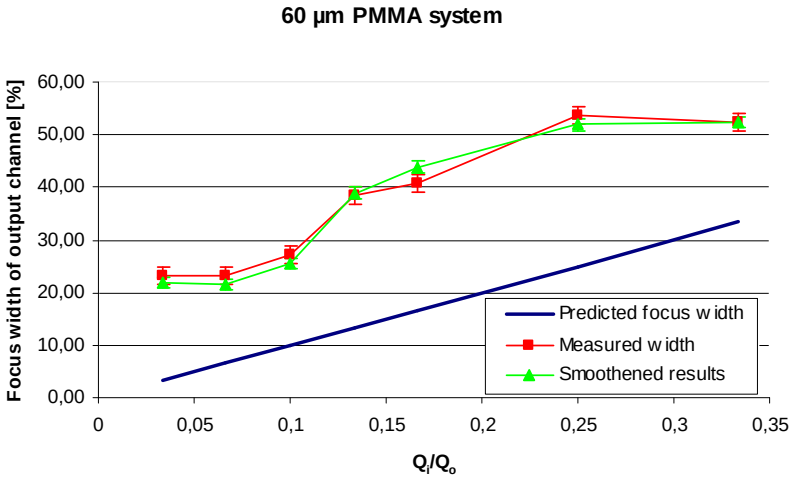

Figure 4-12 – Flow measurements on 60x60 µm PMMA channel system

Measured values on this system were generally higher than predicted. They follow the slope of the predicted curve rather well, and the manual measurements also follow the smoothened values within the possible error overlap on all measurements.

A suspicion as to the reason for the wider focus than expected can be difficulty with achieving strong enough fluorescence to clearly distinguish the focus stream. The objective might have been a little out of focus due to this lack of light, broadening the apparent width of the focus channel. Inverted measurements had been very useful to estimate the average measurements, but unfortunately the prototype connectors did not withstand the pressure long enough to perform these measurements.

4.2.3 100 µm PMMA system

The 100x100 µm PMMA system was the second prototype produced with just one 30x100 µm aperture, and also the second and only other PMMA system in which hydrodynamic focusing was successfully achieved. In this system both ordinary measurements with the fluorescent fluid in the centre channel and inverted measurements were made.

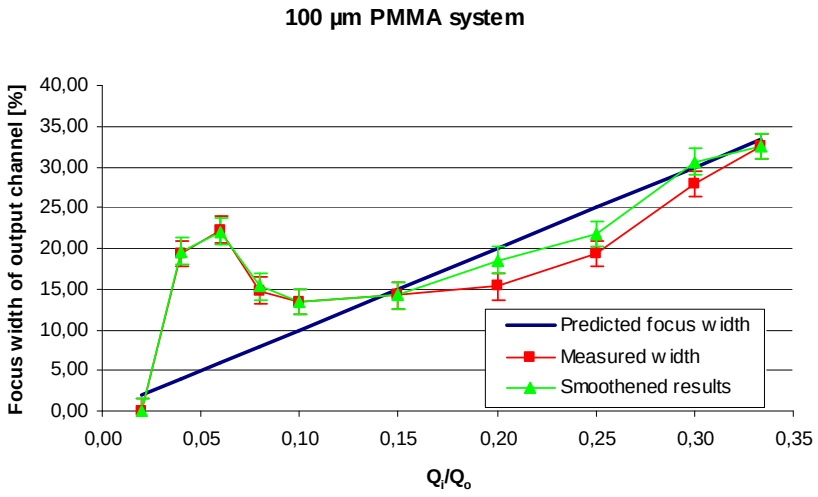

Figure 4-13 – Flow measurements on 100x100 µm PMMA channel system

The ordinary measurements illustrated on the plot of Figure 4-13 indicate problems focusing the centre channel below a certain width, approximately 13,5 % of the output width. The pictures analyzed for the first measurement, predicted to have a width of 2 % of the output channel, does not show a focused stream at all, and as such the value is set to 0 %. From a predicted channel width of 15 % of the output channel and upwards, the measured values are not too far from the predicted values – especially the values coming from the filtered data.

Inverted measurements on the same system are shown on Figure 4-14. The main motivation for performing inverted measurements is due to the less well-defined focus stream edges achieved on the prototype systems, both PMMA and SI systems. A system should give similar results whether the fluorescent fluid is in the centre stream or the sheath flows, so the measurement data should theoretically be more or less negative of each other. By measuring the width of focus channels in both configurations, the values shouldn't vary much, and by meaning the two results the best result should be achieved.

The plot of the inverted measurements is not exactly a clone of that of the initial measurements, but the results tend to follow the same curve shape as those much of the way. The measured values are again furthest from the predicted results for narrower focusing, whereas from approximately 20-25% of the output channel width and upwards they follow the predicted line – except this time a little above the channel instead of a little below it.

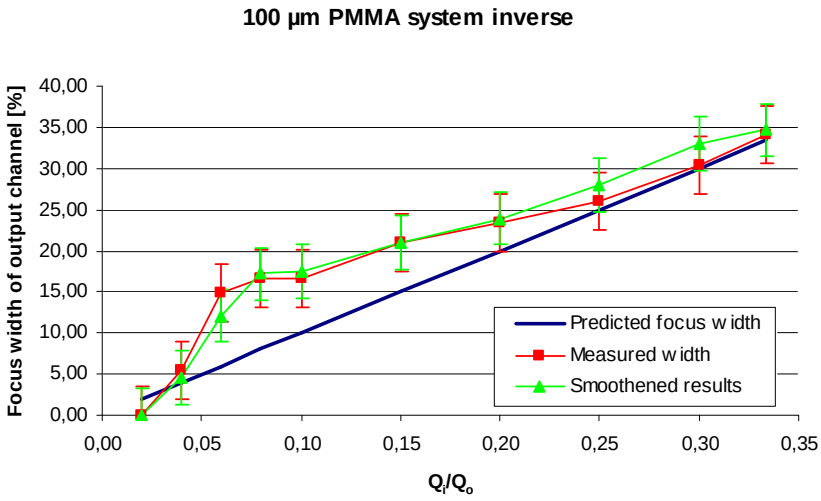

Figure 4-14 – Flow measurements on 100x100 µm PMMA channel system with fluorescent sheath flow

What becomes really interesting is when observing the mean value of the original and the inverted measurements (**Figure** 4-15). Focusing below the range of 13-15% of the output channel width appears as very difficult to achieve with this system, so with an output channel width of 100 µm the range interesting for the Lab-on-a-Chip project is really out of the question. However, between 15 and 33% of the channel width the results follow the predicted system very well. If this could be shown to be the case even after scaling the system down, a control with this precision would be ideal.

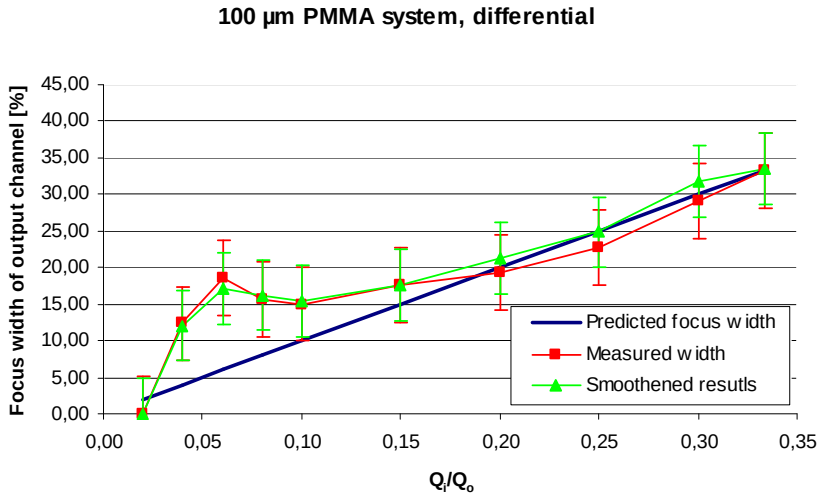

Figure 4-15 – Average values of 100x100 µm PMMA system measurements – non-inverted and inverted

The error bars of course can not be ignored, and could affect the system greatly. Their value on this plot is the sum of the values of those from the averaged measurements, which makes them unnecessary high.

4.2.4 100 µm silicon system

A silicon prototype system with 100x100 µm output channel cross-section has been produced by Bjarke Jacobsen in a project similar to this one. The experiments on this system have been performed using the same laboratory setup, image processing software etc. as for the project at hand. Results have been treated the same way, and are thus directly comparable when presented as on these pages where all focus dimensions are given in a percentage of the output channel width. In this way prototypes with different output channel widths can still be compared directly on their ability to focus a sample inlet down to a certain width.

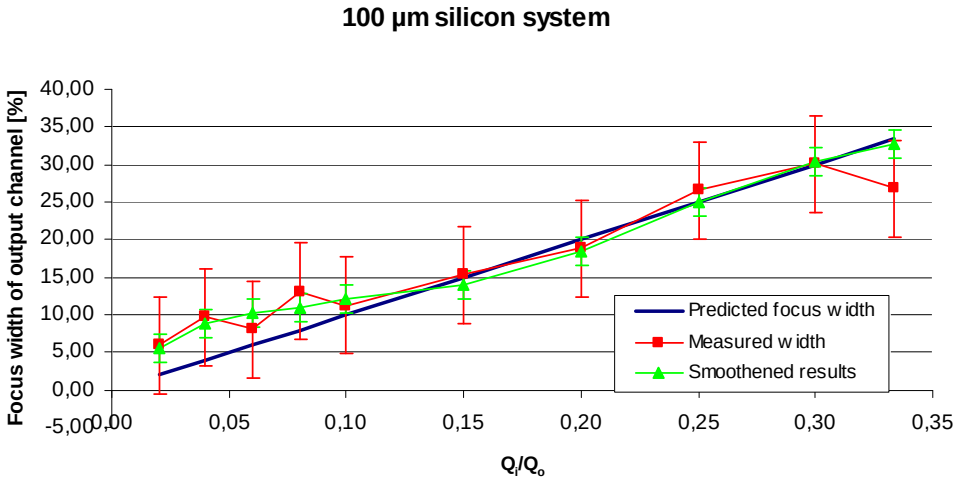

Figure 4-16 – Flow measurements on 100x100 µm silicon channel system

The plot on Figure 4-16 shows a system that for most measurements is rather close to the predicted focus width. From approximately 15% of the output channel width and up to 30%, the measured values are very close to the predicted values, whereas for the areas below 15% of the output channel width results are a little higher than predicted. The results measured without filtering of the signals indicate that measurements were difficult to repeat with high accuracy due to a very rough gradient profile. Filtering of this profile enables much higher precision and repeatability of the measurements, as the error bars also clearly show.

Results from the same prototype tested with inverse fluorescence can be seen on the plot on Figure 4-17. These results are lower than predicted for every value above approximately 5%. The only characteristics shared by the non-inverted and the inverted measurements are their tendency to be higher than the predicted values for attempted focusing with a width of less than 5% of the output channel. Experimental images used for measuring the focus width from inverted measurements show a smaller measurement error than those of the regular measurements. This is mainly due to the higher amount of light coming from a channel containing more fluorescent fluid, in turn giving images with higher contrasts and thus easier identifiable channels.

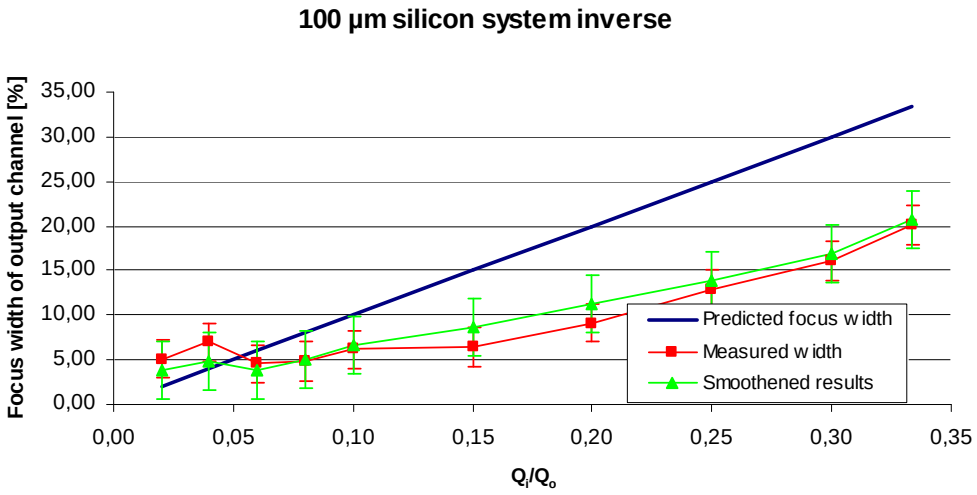

Figure 4-17 – Flow measurements on 100x100 µm silicon channel system with fluorescent sheath flow

Even if the non-inverted and the inverted measurement results appear far from each other, they can be combined to create a graph showing the average measurement values. This graph is shown on Figure 4-18. Average values are in general better for achieving focusing in the range up to approximately 10% of the channel range, in this system 10 µm. Focusing below 5% of the channel range could has not been achieved. The measurements, especially those made after filtering the gradient profiles, follow an almost straight line intersecting the "Predicted width" line at around 7,5% output channel width, but has a lower slope than the predicted line.

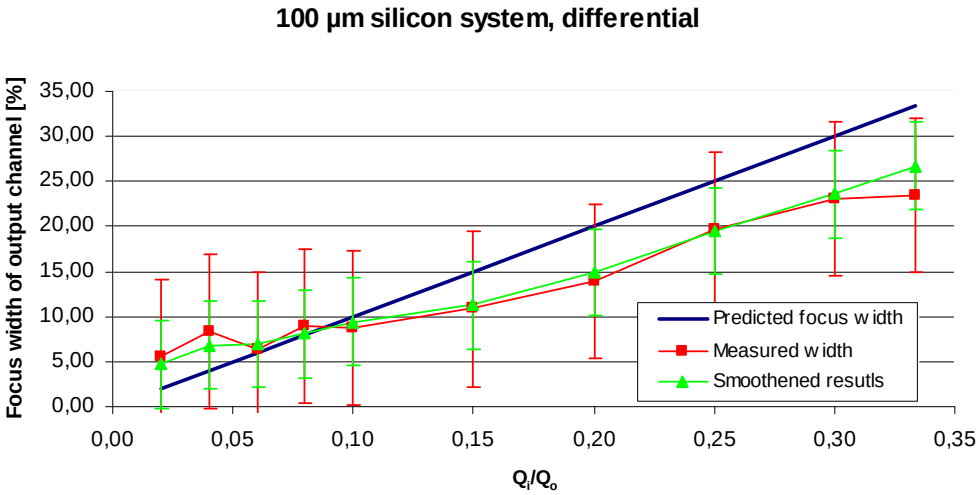

Figure 4-18 Average values of 100x100 µm silicon system measurements – non-inverted and inverted

The error bars on the averaged measurement chart are very large due to the summation of errors from 2 sets of measurements. Performing the same measurement a number of times would likely have decreased this error size, as errors are estimated between only two sets of measurements performed on the same data, but further iterations of data analysis were not achievable within the time scope of the project.

4.2.5 System comparison

Estimating the performance of the different systems on which experiments has been executed is key to determine which method that produced the best results. The difference between the direct measurements and the filtered results are generally close, with the filtered results believed to be a little more precise in terms of repeatability and thus smaller measurement errors. Comparing the commercial system to the averaged measurements from the 100 µm silicon system and the 100 µm PMMA system is done in Figure 4-19, and the filtered values are compared in Figure 4-20.

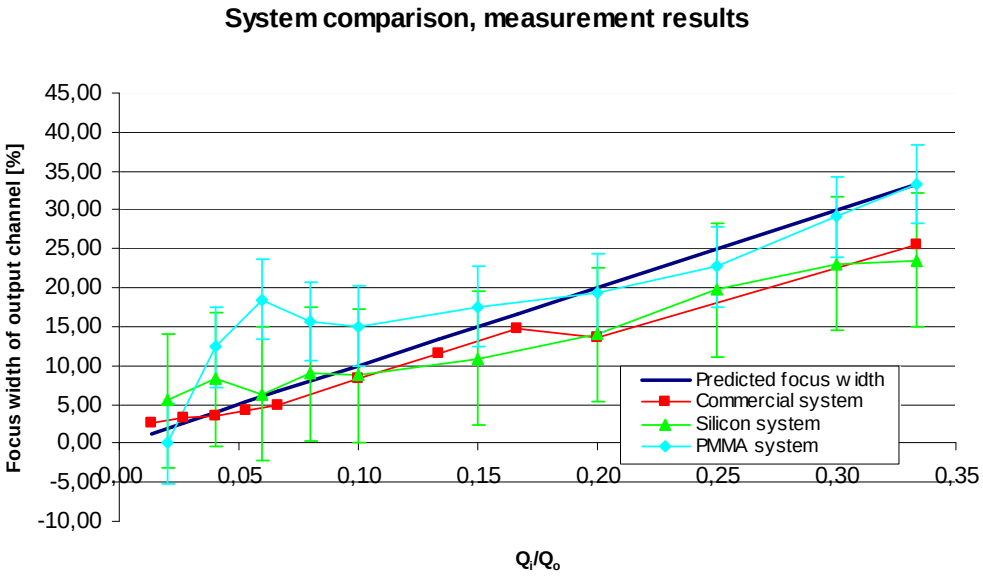

Figure 4-19 – Comparison of commercial system, silicon system and PMMA system – measured results

In the low focusing range, below 15% of the output channel width, the commercial system and the silicon system display better results than the PMMA system. As the low range focusing is what is intended for use in the larger Lab-On-a-Chip project, these results suggest that the silicon system is favourable to the PMMA system. For the smallest focus channel sizes, below 5% of the channel width, the commercial system is better than both prototype systems. As previously discussed, the PMMA system is good for achieving focusing close to the predicted focus at higher values, but these ranges are less relevant for this particular project.

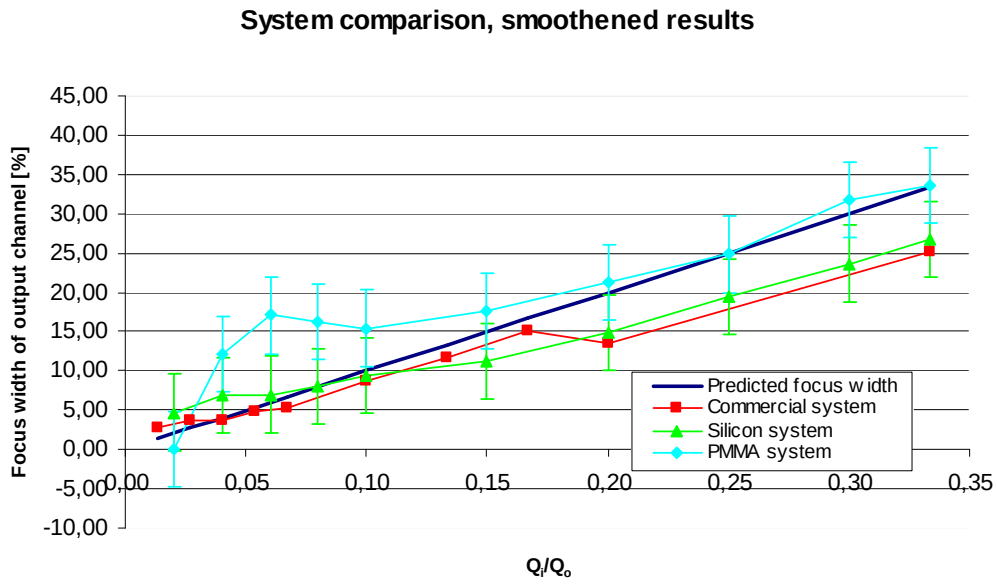

Figure 4-20 – Comparison of commercial system, silicon system and PMMA system – smoothened results

The smoothened results are very close to those without filtering. The silicon system shows a more linear profile than both the other systems, but the commercial system is still better than both prototypes for all low-range focusing.

4.2.6 Focusing conclusions

Performance of the commercially available system is in general better than that of the prototypes performed in this project. The prototypes produced in silicon in the concurrent project also show better focusing in the lower size range which is what is interesting for the larger Interreg4A project.

Performing measurements on both prototype systems has been very challenging. The transparent nature of the PMMA enabled lighting from behind the structures with white light, making the channel structures more easily visible but with the risk of decreasing the visible difference between fluorescent and non-fluorescent fluid channels.

Measurement errors occur mainly due to the difficulty in interpreting precisely enough images of focused streams which do not stand out very clearly to the sheath flow streams. Filtering of the data can improve this to some extent, but subsequent measurements to determine errors still resulted in large measurement errors, especially for the non-transparent silicon prototype. A better approach would likely be to perform a series of consecutive analysis on the same image data, and determine the mean measured values and the error from this data, but time constraints has not allowed that process in this project.

5. Conclusion

The purposes of the project have been met to a certain degree. Production of a number of prototypes has been performed, using a mask and a “stitching” method, which proved extremely time-consuming.

Issues regarding the sealing of and interfacing to the produced prototypes were many – clogged channels, releasing lamination seal, leaking connectors etc. The process from starting with a blank PMMA sample until having a working prototype is long, and many things must be considered in order to experience success.

Sealing with ARcare 7815 tape, interfacing holes cut prior to application, proved to be the best sealing method tested. Homemade connectors in PDMS are challenging to attach, and subject to leaking or breaking if the pressure becomes too high, but working with them has given experience and in combination with a silicone sealing around the attached connectors they give good results.

Achieved focusing in the prototypes did not live up to the desired control – less than 5 µm focus width was not achieved on either of the PMMA prototypes, and controlling the focus below 15 µm is very difficult. A distorted channel cross-section is probably part of the reason for this, an inhomogeneous focused laser spot during production likely to blame.

The silicon prototypes were better for controlling focus in the low range, but neither of the prototypes performed as well as the commercial system, which could be controlled down to a focus width of around 4 µm.

For future prototype production use of the laser is not recommended, at least not with a “stitching” approach. Ablation of an entire system with one aperture is less time-consuming, but at the same time gives less control of the channel depth exactly at the focus point. This did not appear to cause any problems regarding the operation of the system though.

Manufacturing directly in silicon, which has been done by Bjarke Jacobsen in a parallel project, gives rise to many problems in observing the finished system due to the opaque nature of silicon. Channel dimensions and cross-section profile are however much more controllable and uniform using this approach.

Observation of the focusing has proven to be a big issue. 2 different setups were tested with varying success, but neither resulted in very good image quality. As the focusing itself is not what is desired to observe in the Interreg4A Lab-On-a-Chip project, this might not be that big of an issue, but regarding further development and tuning of production of a focusing system it should be considered.

Various sources ([13]+[14}) have had success with producing their entire channel system in PDMS by first using standard lithography to build a negative structure in resist upon a silicon wafer, and then molding the PDMS directly on this structure. Sealing these systems can be done mechanically by squeezing them between glass plates or applying a smooth PMDS “plate” on top. Due to the ease of making holes to interface tubing directly into the PDMS connectors, and general ease of working with PDMS, this approach is believed to be worth examining for further use in the Interreg4A project.

6. Bibliography

[1] **Project description of the Interreg4A Lab-on-a-chip project (in Danish or German)**
http://www.interreg4a.dk/wm242732 (Danish)
http://www.interreg4a.de/wm243034 (German)

[2] **Paul A. Tipler, Gene Mosca: Physics for scientists and engineers, 5th ed. ,**
ISBN 0-7167-4389-2, W.H.Freeman and Company, 2003

[3] **Dirk Bastin, Gerd Marowsky (Eds.): Excimer Laser Technology**
ISBN-10 3-540-20056-8, Springer-Verlag Berlin Heidelberg, 2005

[4] **H-G. Rubahn: Laser Applications in Surface Science and Technology**
ISBN 0-471-98450-7. Wiley-VCH, 1999

[5] **K. Naessens, S. Boons, A. V. Hove, T. Coosemans, S. Verstuyft, H. Ottevaere, L. Vanwassenhove, P. V. Daele and R. Baets: Excimer laser ablated U-groove alignment structure for optical fibre arrays**
ISBN 2-9600226-0-2, p. 187-190, 1999

[6] **Yunus A. Çengel, Robert H. Turner: Fundamentals of Thermal-fluid sciences, 2nd ed.**
ISBN 007-123926-X, McGraw-Hill int. ed., 2005

[7] **T. Stiles, R. Fallon, T. Vestad, J. Oakey, D. W. M. Marr, J. Squier, R. Jimenez: Hydrodynamic focusing for vacuum-pumped microfluidics**
Microfluid. Nanofluid. 1: 280-283, 2005

[8] **Stephen D. Senturia, Microsystem Design**
ISBN 0-7923-7246-8, Kluwer Academic Publishers, 2000

[9] **Image source:**
(a) Datasheet received from manufacturer on inquiry
(b) Online product catalog from www.microfluidic-chipshop.com

[10] **Abdirahman Yussuf, Igor Sbarski, Jason Hayes, Matthew Solomon: Sealing and Bonding Techniques for Polymer-Based Microfluidic Devices**
http://www.swinburne.edu.au/feis/iris/pdf/profiles/AbdirahmanYussuf.pdf

[11] **Daniel Olivero, Z. Hugh Fan, Lamination of Plastic Microfluidic Devices**
http://www.rsc.org/Publishing/Journals/lc/Chips_and_Tips/lamination.asp

[12] **Swomitra Mohanty, David J. Beebe: PDMS connectors for macro to microfluidic interfacing**
http://www.rsc.org/Publishing/Journals/lc/PDMS_connector.asp

[13] **T. Stiles, R. Fallon, T. Vestad, J. Oakey, D. W. M. Marr, J. Squier and R. Jimenez (2005): Hydrodynamic focusing for vacuum-pumped microfluidics**
Microfluidics and Nanofluidics, 1, p. 280-283. ISSN 1613-4990.

[14] **Gwo-Bin Lee, Chih-Chang Chang, Sung-Bin Huang and Ruey-Jen Yang (2006): The hydrodynamic focusing effect inside rectangular microchannels**
J. Micromech. Microeng. 16 (2006) 1024-1032.

[15] **Nam-Trung Nguyen, Yit-Fatt Yap and Agung Sumargo (2008): Microfluidic rheometer based on hydrodynamic focusing**
Meas. Sci. Technol. 19 (2008) 085405 (9pp)

7. Appendix index

1. Flow resistance calculation graph

System	Channel	L	w	h	R	Q	ΔP		
		mm	µm	µm	Pa·s/m^3	µl/min	Pa	atm	
Commercial	Input	23	60	60	1,90E+13	125	3,95E+04	3,90E-01	
	Sheath	13	100	100	1,39E+12	185	4,28E+03	4,22E-02	
	Output	49	150	100	3,49E+12	375	2,18E+04	2,15E-01	
Intended 1	Input	25	50	100	5,34E+12	83,33	7,42E+03	7,32E-02	
	Sheath	29	50	100	6,19E+12	122,50	1,26E+04	1,25E-01	
	Output	35	100	100	3,74E+12	250,00	1,56E+04	1,54E-01	
Proto1	Input	25	30	100	8,90E+12	50,00	7,42E+03	7,32E-02	
Stitching 1	Sheath	29	30	100	1,03E+13	72,50	1,25E+04	1,23E-01	
	Output	35	60	100	6,23E+12	150,00	1,56E+04	1,54E-01	
Proto2	Input	15	30	60	2,47E+13	50,00	2,06E+04	2,03E-01	
Stitching 2	Sheath	19	30	60	3,13E+13	72,50	3,78E+04	3,73E-01	
	Output	25	60	60	2,06E+13	150,00	5,15E+04	5,08E-01	
Proto3	Input	15	60	60	1,24E+13	50	1,03E+04	1,02E-01	
60 µm	Sheath	19	60	60	1,57E+13	72,5	1,89E+04	1,87E-01	
	Output	25	60	60	2,06E+13	150	5,15E+04	5,08E-01	
Proto4	Input	15	100	100	1,60E+12	83,33	2,23E+03	2,20E-02	
100 µm	Sheath	19	100	100	2,03E+12	122,5	4,14E+03	4,09E-02	
	Output	25	100	100	2,67E+12	250	1,11E+04	1,10E-01	

2. Mask data sheet

Nanofilm

Specification Data Sheet

Substrate Material Specifications

Parameter	Substrate Material			
	Green Soda Lime (SL)	White Crown (270)	Borofloat	Quartz (QZ)
Composition (%)				
$Si0_2$	73	70	60	100
B_2O_3	-	-	5	-
Al_2O_3	1	-	15	-
Na_2O	15	8	1	-
K_2O	1	9	1	-
RO	10	14	18	-
Thermal Properties				
Coefficient of Expansion Over 50-200°C	94 X 10^{-7}/°C	93 X 10^{-7}/°C	37 X 10^{-7}/°C	4-5 X 10^{-7}/°C
Softening Point (°C)	740	710	900	1600
Transformation Temp. (°C)	562	520	673	-
Strain Point (°C)	511	505	636	1000
Optical Properties				
Light Transmittance (%) d=2.3mm, λ=400nm	90	91	91	90 (λ=400nm)
Refractive Index (n_d)	1.52	1.52	1.53	1.46
Chemical Properties (Weight Loss mg/cm2)				
Water (25°C/4h)	1.2 X 10^{-3}	1.2 X 10^{-3}	8.0 X 10^{-4}	8.0 X 10^{-5}
NaOH 5% (100°C/6h)	1.1	1.1	1.4	0.9
HCl 5% (80°C/1h)	1.0 X 10^{-2}	1.0 X 10^{-2}	5.0 X 10^{-3}	4.0 X 10^{-4}
Mechanical Properties				
Specific Gravity	2.49	2.55	2.58	2.20
Young Modulus (kg/mm^2)	7000	7340	7540	7413
Sheer Modulus (kg/mm^2)	2870	2980	3260	33170
Knoop Hardness (kg/mm^2)	540	530	657	615
Electrical Properties				
Bulk Resistivity at 200°C	7.7	9.6	10.6	12.5
Dielectric Constant at IMH, R.T.	7.5	7.1	6.1	4.0

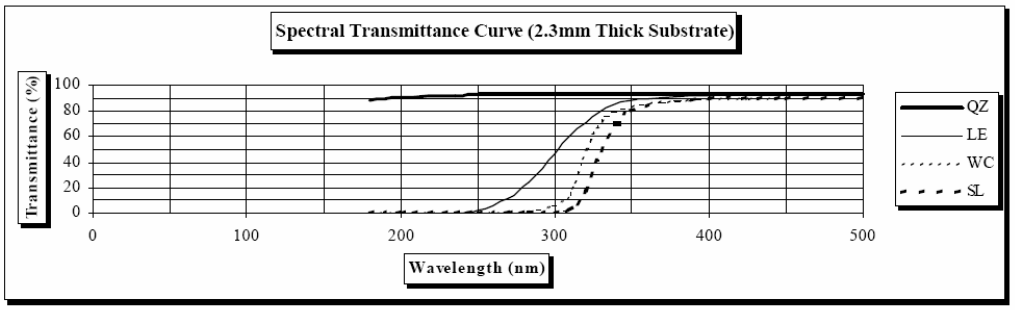

2641 Townsgate Rd. ◆ Westlake Village, CA ◆ 91361 ◆ www.Nanofilm.com ◆ TEL: 805-496-5031 ◆ FAX: 805-373-9393

Data about the mask ordered for prototype fabrication. The ordered mask was a Quartz glass to ensure transparency at 193 nm.

3. ARcare 7815 sealing tape datasheet

PRODUCT DESCRIPTION

ARcare® 7815 is a clear, thin and flexible plastic film coated on one side with a medical grade pressure-sensitive adhesive. The adhesive side of the tape is protected by a clear siliconized polyester release liner.

FEATURES

- Non-migratory acrylic adhesive
- Inert acrylic adhesive
- Flexible adhesive system
- Easily die cut
- Tolerant to Gamma sterilization

BENEFITS

- Allows lateral flow in membrane- based devices
- Compatible with many assays
- Excellent conformability
- Facilitates design options
- Suitable for sterilization processes

PRODUCT PROFILE

Substrate:	2 mil clear polyester film
Adhesive:	AS-110 acrylic medical grade adhesive
Liner:	2 mil clear siliconized polyester release film

PROPERTIES

ATTRIBUTE	NOMINAL VALUE*
180° Peel Adhesion:	40 oz/in. minimum
Optical Properties:	95.9% Light Transmission
Coat Weight:	0.95 oz./yd.²
Thickness Without Liners:	3.0 mils
Total Thickness:	5.0 mils

***All stated values are nominal and should only be used as a guide for selection.**

PRODUCT APPLICATIONS

This product is suggested for bonding, laminating and assembly of in-vitro diagnostic and related membrane-based immunoassay products. It is necessary, as with all pressure-sensitive tapes, that the surface to which the tape is to be applied be clean and dry.

SAFETY DATA

AS-110 is an acrylic, pressure-sensitive adhesive. The adhesive passed cytotoxicity and primary skin irritation tests conducted by an independent laboratory. Additional safety information is available by accessing our Drug Master Files or Device Master Files.

Product Information

ARcare® 7815

Clear Polyester Film

Insight℠ Adhesives Research

STORAGE

Unconverted rolls should be stored at 70° F (21° C) and 50% relative humidity, out of direct sunlight.

PRODUCT PROFILE AND DIAGRAM

(MEDPI – 06/27/05)

STORAGE OF PRESSURE-SENSITIVE ADHESIVE TAPES

Pressure-sensitive adhesive tapes function as a mechanical product; however, the adhesive itself is a chemical composition that can be sensitive to environmental conditions. A purchaser of pressure-sensitive adhesive products should be aware of the shelf life of each product and not purchase more than it can use before the expiration date. Shipping and storage conditions affect shelf life. The optimum storage temperature is 70°F (21°C). Cool, dry storage is recommended.

For best results...

1) The surfaces you wish to bond should be clean and free of oil, moisture and dust. If the surface temperature is below 40°F, it may be difficult to achieve a proper bond.
2) Do not use a pressure-sensitive adhesive product where it will be exposed to temperatures lower or higher than those designated for each product. Heat can destroy the effectiveness of the bond and extreme cold can cause the adhesive to harden and not adhere properly.
3) When the tape is applied, use firm hand or lamination pressure to achieve contact between the adhesive and the surface to which it is applied. Hand rollers or nip rollers may be needed for certain products or applications.

Consult your AR sales representative if you need additional information.

DISCLAIMER

AR expressly warrants to Purchaser that its product, under normal and intended use maintenance and storage, is free from defects in workmanship for twelve (12) months from the date of shipment, unless otherwise stated. THIS WARRANTY IS GIVEN IN LIEU OF ALL OTHER WARRANTIES. **AR MAKES NO WARRANTY AS TO EXPERIMENTAL AND DEVELOPMENTAL SAMPLES OR MATERIALS. AR MAKES NO WARRANTY OF MERCHANTABILITY OR FITNESS FOR A PARTICULAR PURPOSE.** No provisions, representations, diagrams, drawings or pictures contained in any product literature, price list, catalogue, purchase order, product data sheet, order acknowledgment, invoice, delivery ticket, or any other communication by AR, including information on AR's website or representations made by AR's employees or agents, constitute express warranties. Results of tests and recommendations included in communications of AR do not constitute express warranties. SINCE MANY FACTORS MAY AFFECT THE USE AND PERFORMANCE OF AN AR PRODUCT IN A PARTICULAR APPLICATION, INCLUDING, AMONG OTHERS, THE PRODUCT SELECTED FOR USE, THE CONDITIONS IN WHICH THE PRODUCT IS USED, THE TIME AND ENVIRONMENTAL CONDITIONS IN WHICH THE PRODUCT IS EXPECTED TO PERFORM, THE MATERIALS TO BE USED WITH THE PRODUCT, THE SURFACE PREPARATION OF THOSE MATERIALS, AND THE APPLICATION METHOD FOR THE PRODUCT, PURCHASER ACCEPTS RESPONSIBILITY FOR DETERMINING WHETHER AR'S PRODUCT IS FIT FOR A PARTICULAR PURPOSE AND SUITABLE FOR PURCHASER'S METHOD OF APPLICATION. AR retains the right to modify or change its products if in AR's judgment it is advisable.

Purchaser's exclusive remedy and AR's sole obligation for any breach of warranty is limited to, at AR's option, either: 1) replacement of AR's product, or 2) reimbursement of the purchase price of AR's product. **AR DISCLAIMS ANY OTHER OBLIGATION OR LIABILITIES ARISING OUT OF BREACH OF WARRANTY.** AR will not be liable of any loss, damage, expense or consequential, incidental or special damages of any kind.

Internet: www.adhesivesresearch.com

Adhesives Research, Inc.
400 Seaks Run Road, P.O. Box 100
Glen Rock, PA 17327
Toll-free: 800-445-6240
Phone: 717-235-7979
Fax: 717-235-8320

Adhesives Research Ireland Ltd.
Raheen Business Park, Limerick, Ireland
Phone: +353 61 300 300
Fax: +353 61 300 700

Adhesives Research Ltd.
The Old Exchange, Mill Lane
Great Dunmow, Essex, UK CM6 1BG
Phone: +44 (0)1371 856300
Fax: +44 (0)1371 856380

Adhesives Research Pte. Ltd.
20 Maxwell Road
#12-08B Maxwell House
Singapore 069113
Phone: +65 6774 9580
Fax: +65 6777 7261

Adhesives Research Shanghai Representative Office
Suite 3908, Plaza 66 Tower 1
1266 Nanjing West Road
Shanghai, China 200040
Phone: +86 21 61038526
Fax: +86 21 61038527

Adhesives Research GmbH
Stefan-George-Ring 29, D-81929
München, Germany
Phone: +49 (0) 89 930 86 220
Fax: +49 (0) 89 930 51 84

For further information about the sealing tape or other products, please look on http://www.adhesivesresearch.com

4. Würth 180 special silicone brochure

WÜRTH

THE ASSEMBLY PROFESSIONALS

Silicone Special 180

Colour: transparent
- Temperature resistant from -50°C up to 150°C, short term up to 180°C.

Contents	Art. No.	Pack Qty.
100g/70ml	**0890 320**	10/1

Silicone Special 250

Colour: red
- Temperature resistant from -50°C up to 250°C, short term up to 300°C.

Contents	Art. No.	Pack Qty.
100g/70ml	**0890 321**	10/1

Silicone Special

- Cold vulcanising silicone rubber.
- Permanently elastic silicone sealing compound for engine and body.
- For sealing of surfaces, gaps and cracks on water pumps, oil sumps radiators, crank cases etc.
- Bridges large, uneven surfaces.
- Gives a reliable seal, withstanding many years of vibration.
- Excellent adhesive properties.
- Will not drip, sag or become stringy.
- Excellent chemical resistance.
- Skin formation after a few minutes, vulcanisation rate approx. 1.5mm/day.

Application

Sealing joints, cylinder head, crank case, water pump, oil sump, radiator, gear box, axle housing, cylinder casing (motorcycles), lamp and direction indicator housings, welding seams etc.

DP 300

universal gasket jointing compound

Colour: blue
- Manufactured under license from Rolls Royce Ltd.
- Permanently elastic sealing compound for engine and body.
- Gives a reliable seal, withstanding many years of vibration.
- Excellent adhesive properties.
- Will not drip, sag or become stringy.
- Temperature resistant from -50°C to 300°C
- Minor conduction of heat.
- Will not react with metal or other materials.
- Resistant to water, air, petrol, kerosine oil, synthetic lubricants, water/glycol and methanol mixtures, anti-freeze cooling agents, flurocarbon cooling agents.
- Do not use instead of solid gasket.
- Do not use on oil pans.
- Silicone free.

Contents	Art. No.	Pack Qty.
100g/80ml	**0890 100 048**	10/1

UK/gw - 07/08 - 0214 - ©

This information is intended as a recommendation only, based on our experience. Preliminary tests to verify material compatibility should be carried out. The cleaning and care instructions of the manufacturer must be observed!

06 0216

Source: http://www.wurth.co.uk/catalogue/pdfs/UK-CD_06_0216.pdf

5. Trypan blue Product Information Sheet

Product Information Sheet

TRYPAN BLUE
0.4% (w/v)

Catalog # 07050 **100 mL/bottle**

FORMULATION:

0.4% trypan blue in phosphate buffered saline

STABILITY / STORAGE:

Stable for at least two years when stored at room temperature.

Contents guaranteed sterile if seal is not tampered with.

DIRECTIONS FOR USE:

For viable cell counts of mammalian cells. Dilute the cells 1:1 in trypan blue. If the cell count appears high, the cells may first be diluted with a balanced salt solution before trypan blue is added . Allow the resulting solution to sit for 5 - 15 minutes. Only non-viable cells will stain with the trypan blue dye; viable cells will remain unstained. Note: If cells are incubated for greater than 15 minutes in trypan blue, toxicity effects may occur and the viable cell count will be inaccurate.

Prepare a hemocytometer by first cleaning the chamber surface with alcohol. Wipe dry. Position the cover-slip over the chambers. Carefully transfer sufficient volume of the trypan blue/cell solution to each chamber using a capillary tube or pipetman. Do not over- or underfill. Begin by counting the cells on one chamber. Keep a separate count of viable (unstained) and non-viable (blue) cells. Count all cells in each 1 mm square (see Figure 1) of each chamber. If cells are on the border outlining each square, count only the cells on the top and left border of the square. Note: Each square has a total volume of 0.1 mm^3 (or 10^{-4} cm^3 which is approximately equivalent to 10^{-4} mL).

Determine the cell count (cells per mL) as follows:

AVERAGE CELL COUNT PER SQUARE x DILUTION FACTOR x 10^4
= CELL COUNT PER ML

Determine the cell viability (%) as follows:

$$\frac{\text{CELL COUNT (VIABLE)}}{\text{TOTAL CELL COUNT (VIABLE + NON-VIABLE)}} = \text{CELL VIABILITY (\%)}$$

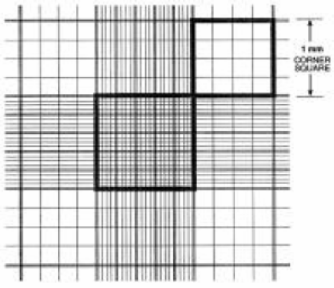

Figure 1. Neubauer hemacytometer showing dimensions of each square. Depth = 0.1 mm

THIS REAGENT IS FOR LABORATORY USE ONLY.
IT IS NOT TO BE ADMINISTERED TO HUMANS.

Hazardous Ingredients: *Avoid ingestion, exposure to skin and eyes. Wash exposed skin with soap and water. Flush eyes with water. See Material Safety Data Sheet for additional information.*

STEMCELL TECHNOLOGIES INC
777 West Broadway, Suite 808
Vancouver, British Columbia
CANADA V5Z 4J7

Revised July 2002
Tel: (604) 877-0713 Toll-free Tel: 1-800-667-0322
Fax: (604) 877-0704 Toll-free Fax: 1-800-567-2899
Website: www.stemcell.com E-mail: info@stemcell.com

Source: http://www.stemcell.com/technical/07050-PIS.pdf

6. Hamilton syringe specification sheet

HAMILTON
THE MEASURE OF EXCELLENCE™

(80931) 1705RNCP 50ul SYR (22s/.75"/3)

Product Specifications

Volume	50 µL
Termination	RN
Syringe Type	GASTIGHT
Syringe Series	1700
Std. Needle Dead Volume	.90 µL
Sales Quantity	1 syringe per pack
Point Style	3
Outer diameter	0.028 inch (0.7 mm)
Needle	Small RN
Minimum Temperature	10° C / 50° F
Maximum Temperature	115° C / 239° F
Maximum Pressure	1000 psig (68.9 bar)
Max. Temp. w/ Cemented Needle	50° C / 122° F
Length	0.75 inch (19.1 mm)
Inner Diameter	0.006 inch (0.2 mm)
Gauge	22s gauge
Gas Sterilized	Yes
Fluid Path	SST, Borosilicate glass, PTFE
Autoclavable	Yes

Source / more information on: http://www.hamiltoncompany.com/products/syringes/c/796/